Distribution Agreement

Ruth Nelson April 10, 2023

Age-Dependent Changes in Perineuronal Nets and Associated Parvalbumin Interneurons in the 5XFAD Amyloidosis Mouse Model

by

Ruth Nelson

Srikant Rangaraju
Adviser

Neuroscience and Behavioral Biology

Srikant Rangaraju

Adviser

Joseph Manns

Committee Member

Kevin McAlister

Committee Member

2023

Age-Dependent Changes in Perineuronal Nets and Associated Parvalbumin Interneurons in the 5XFAD Amyloidosis Mouse Model

By

Ruth Nelson

Srikant Rangaraju

Adviser

An abstract of
a thesis submitted to the Faculty of Emory College of Arts and Sciences
of Emory University in partial fulfillment
of the requirements of the degree of
Bachelor of Science with Honors

Neuroscience and Behavioral Biology

2023

Abstract

Age-Dependent Changes in Perineuronal Nets and Associated Parvalbumin Interneurons in the 5XFAD Amyloidosis Mouse Model

By Ruth Nelson

Perineuronal nets (PNNs) are extracellular matrix structures that surround neurons and proximal dendrites and regulate synaptic transmission, plasticity, and several facets of memory. PNNs are commonly associated with parvalbumin-positive (PV+) fast-spiking interneurons which are hypothesized to play physiological roles in memory and cognition. Despite a growing literature related to PNNs and PV+ neurons' roles in synaptic maintenance and memory, much remains unknown regarding how these structures are affected in neurodegenerative diseases such as Alzheimer's Disease (AD). In this study, we used the 5XFAD amyloidosis mouse model to investigate how AD-like pathology affects PNNs and PV+ neurons. Using immunofluorescence microscopy, we stained 5XFAD and Wild Type (WT) mice at 1.8, 3, 6, and 10 months of age. We stained for PV+ neurons, PNNs, and for Amyloid-Beta (Aβ) plaques. Images were then processed using ImageJ to quantify the presence of PV+ neurons, PNNs, and the association between them in several regions of interest across genotypes and age groups. We found that PNNs, but not PV+ neurons, are significantly depleted in the anterior cortex, posterior cortex, and subiculum of the 5XFAD mice in early amyloidosis (3-6 month old 5XFAD mice). Furthermore, analyses investigating the co-localization of PNNs and PV+ neurons in these regions found that PNNs were depleted surrounding PV+ neurons in an age-dependent manner in the 5XFAD mice compared to WT. Specifically, in early amyloidosis (3-6 months) there was a general depletion of PNNs, but in later amyloidosis (6 -10 months) the depletion of PNNs was preferentially surrounding PV+ neurons. Finally, assessing the relationship between Aβ plaque proximity and the co-localization between PNNs and PV+ neurons revealed that PNNs closer to Aβ plaques were more likely to be associated with PV+ neurons. Collectively, these findings may indicate the time-dependent impact of Aβ pathology on PNNs, both in general and specifically surrounding PV+ neurons.

Age-Dependent Changes in Perineuronal Nets and Associated Parvalbumin Interneurons in the 5XFAD Amyloidosis Mouse Model

By

Ruth Nelson

Srikant Rangaraju

Adviser

A thesis submitted to the Faculty of Emory College of Arts and Sciences
of Emory University in partial fulfillment
of the requirements of the degree of
Bachelor of Science with Honors

Neuroscience and Behavioral Biology

2023

Acknowledgements

Thank you very much to Dr. Srikant Rangaraju and Dr. Claudia Espinosa-Garcia who have provided me with invaluable mentorship throughout this process. I would also like to thank the other members of the Rangaraju lab for creating such a warm and supportive lab environment during my time at Emory.

I would also like to thank my amazing friends Joe Lee, Sam Ambarian, Steve Gaunt, Israel Negrete-Abreu, Schuler Arn, and Natalie McGrath. You all have shaped, improved, and brightened this thesis just as you have with every one of my experiences at Emory.

Finally, I would like to thank my family, Peter Nelson, Deborah Nelson, Bela Nelson, Abe Nelson, and Tess Nelson. Your constant love and support mean so much to me.

Table of Contents

Introduction

Alzheimer's Disease (AD) is the leading cause of dementia worldwide, constituting ~70% of all cases and afflicting more than 50 million individuals (Prince et al. 2013; '2020 Alzheimer's disease facts and figures' 2020). As the population ages, the number of affected people is projected to double by the year 2050 (Prince et al. 2016). Clinically, AD manifests as deficits in memory that evolve to encompass global cognitive function and, ultimately, the dementia clinical syndrome. The primary pathological hallmarks of AD are extracellular Amyloid-β (Aβ) plaques and intracellular neurofibrillary tangles (NFTs) (Braak and Braak 1991; Serrano-Pozo et al. 2011).

Along with the disease-specific pathological features, AD brains also demonstrate neuronal death and synaptic loss, both of which correlate with cognitive decline (Subramanian, Savage, and Tremblay 2020). To further understand how AD pathogenesis affects neural circuity, emerging research is looking beyond neurons themselves to Extracellular Matrix (ECM) structures called perineuronal nets (PNNs). These intriguing structures form lattice-like assemblies around the soma and proximal dendrites of neurons in the brain. PNNs form a key part of the "tetrapartite synapse" which regulates synaptic activity along with pre- and post-synaptic terminals and adjacent glial cells (Chelini et al. 2018).

PNN Composition

PNNs are composed largely of Chondroitin Sulfate-Proteoglycans (CSPGs) which are attached to hyaluronan (HA) via link proteins and anchored to the cell via hyaluronan synthase (HAS) proteins (Bekku et al. 2003) (Suttkus et al. 2014). The most common CSPGs found in PNNs are of the lectican family which includes aggrecan (the most common) as well as versican, neurocan, and brevican (Ueno et al. 2018). The CSPGs are covalently associated with

glycosaminoglycan (GAG) side chains which are composed of disaccharide repeating units. The type of GAG side chain and their sulfation states introduce extensive heterogeneity in PNNs and are hypothesized to underlie their function (Scarlett, Hu, and Alonge 2022).

An Overview of PNN Functions

PNNs are proposed to serve many functions in the brain including regulating critical periods of development, synaptic transmission and plasticity, and memory as well as protecting neurons from harmful stimuli (Guimaraes, Zaremba, and Hockfield 1990; Bosiacki et al. 2019). In critical periods of development, which are characterized by increased synaptic plasticity, PNNs are notably absent (Hockfield et al. 1990). Furthermore, the formation of PNNs corresponds to the ending of critical periods and the establishment of mature synaptic connections (Guimaraes, Zaremba, and Hockfield 1990). This suggests that PNNs play a critical role in the stabilizing of neuronal synapses and the hindrance of synaptic plasticity which is necessary for the closing of critical periods of development.

Further, PNNs are proposed to restrict synaptic plasticity by imposing a physical carrier which hinders new synaptic connections, serving as a scaffold for molecules that hinder synaptic connections, and limiting receptor mobility at synapses (Deepa et al. 2002; Corvetti and Rossi 2005; Frischknecht et al. 2009; Sorg et al. 2016). These functions are modulated by the individual components of PNNs. Experimentally degrading individual PNN components can provide insight into the functionality of the individual components and the structure as a whole. Intraparenchymal injection of chondroitinase ABC (ChABC) selectively degrades GAG side chains and is found to cause an increase in axonal sprouting, necessarily increasing plasticity (although the formation of long-lasting synaptic contacts was not found) (Corvetti and Rossi 2005). Further

investigation using ChABC demonstrates that GAG digestion increases the firing rate for fast-spiking inhibitory neurons as well as inhibitory inputs into select neuronal subtypes (Balmer 2016; Favuzzi et al. 2017). Degradation of the CSPG core protein components of PNNs is accomplished via metalloproteases (MMPs) including MMP-1. In vitro exogenous treatment of MMP-1 increases Ca2+ signaling (and thus synaptic transmission) and dendritic arborization in vitro (Allen et al. 2016). Furthermore, in-vivo overexpression of MMP-1 increases dendritic complexity and appears to increase GPCR signaling (Allen et al. 2016). Finally, degradation of HA via hyaluronidase increased extra-synaptic AMPA-type glutamate receptor diffusion and the exchange of synaptic AMPA receptors, implicating PNNs in the stabilization of excitatory synapses (Frischknecht et al. 2009). Further, HA has been found to regulate hippocampal synaptic plasticity via modulation of postsynaptic Ca2+ channels (Kochlamazashvili et al. 2010). Collectively, these findings indicate that several core components of PNNs dynamically contribute to their functionality in synaptic transmission and/or plasticity.

In addition to their hypothesized roles in regulating synaptic activity, PNNs are also thought to protect neurons from neurotoxic stimuli. Most notably, in vivo studies examining the effects of oxidative stress demonstrate that PNNs limit the harmful effects of excessive reactive oxygen species (ROS), in a manner proportional to their “robustness” and maturity (Cabungcal et al. 2013; Suttkus et al. 2012). Furthermore, it is also hypothesized that PNNs are protective against inflammatory cytokines seen in many neurodegenerative diseases including AD (Suttkus, Morawski, and Arendt 2016; Reichelt et al. 2019)

Research investigating PNNs has demonstrated their pivotal roles in the regulation of synapses and their potential to protect neurons from neurotoxic stimuli. Thus, to further

understand the pathogenesis of AD —a disorder in which synaptic connections are damaged or lost— we must understand how PNNs react and contribute to AD pathology.

PNNs and Parvalbumin Interneurons

PNNs are associated with fast-spiking classes of neurons which magnify their roles in neurocircuit function. PNNs are most commonly associated with parvalbumin-positive (PV+) GABAergic interneurons, although they are also found surrounding many other classes of excitatory and inhibitory interneurons (Yamada, Ohgomori, and Jinno 2015; Klimczak et al. 2021; Meszar et al. 2012; Hartig, Brauer, and Bruckner 1992; Morikawa et al. 2017). A recent preprint by Lupori et al. asserts that across the entire brain (there is significant regional variability) 59.1 ± 1.0% of PNNs were associated with a PV+ neuron and 30.4 ± 1.4% of PV+ neurons were surrounded by a PNN (Lupori et al. 2023).

While they comprise a small fraction of CNS neurons, the high excitability and firing rates of PV+ neurons enable them to have profound impacts on neural circuitry (Nahar, Delacroix, and Nam 2021). Through their fast-spiking behavior and a high degree of synaptic connections, PV+ neurons play pivotal roles in regulating the spike-timing of nearby glutamatergic pyramidal neurons (Kim et al. 2016). This regulation is in the form of both direct inhibition and disinhibition circuitry (Tremblay, Lee, and Rudy 2016). Neural activity is also regulated by the neural oscillatory patterns of PV+ neurons. Specifically, gamma oscillations in PV+ neurons have been associated with plasticity, learning, and memory (Wingert and Sorg 2021). Several other studies implicate PV+ neurons in coordinating hippocampal synchrony, reward-seeking behavior, infantile learning, spatial representations, and working memory (Miranda et al. 2022; Sparta et al. 2014; Korotkova et al. 2010).

The activity and functionality of PV+ neurons appear to be closely related to their association with PNNs. Similar to the role of PNNs described above, PV+ neurons are reported to be critical in regulating sensory plasticity. This is accomplished in manners both specific to their association with PNNs and by other mechanisms including gain control which normalizes sensory inputs and "compresses" outputs (Rupert and Shea 2022; Sparta et al. 2014). The effect of PV+ neural oscillatory behavior has also been found to be contingent on PNN association. Specifically, Shi et al. found that reduced activity in PNN-associated PV+ neurons regulated theta oscillations during memory consolidation (Shi et al. 2019).

PNNs influence the activity of PV+ neurons by affecting several of their electrophysiological properties. Several studies have demonstrated that the depletion of PNNs causes an increase in firing rate, a decrease in action potential threshold, an increase in resting potential, and an increase in half-width (Wingert and Sorg 2021; Dityatev et al. 2007; Favuzzi et al. 2017). All these factors cause hyperactivity of PV+ neurons which lead to drastic effects on neural circuitry.

In conclusion, PV+ neurons and PNNs play vast roles in neural plasticity and functionality and the close association between them serves to magnify their respective effects.

PNNs and Memory

In addition to the cellular and molecular functions of PNNs, they are associated with several aspects of learning and memory including associative memory, object recognition, and spatial memory. Two types of associative memory that are affected by PNN degradation are eyeblink conditioning and fear conditioning. Eyeblink conditioning is dependent on neurons in

the deep cerebellar nuclei which are densely surrounded by PNNs (Carulli et al. 2006). Injection of ChABC (which degrades GAG side chains of PNNs) increases the acquisition of eyeblink conditioning but decreases the retention of this response (Carulli et al. 2020). Furthermore, PNN removal in the Basolateral Amygdala (commonly associated with fear conditioning) as well as the hippocampus, medial prefrontal cortex, anterior cingulate cortex, and auditory cortex impairs the expression of fear conditioning (Gogolla et al. 2009; Hylin et al. 2013; Banerjee et al. 2017; Gunduz-Cinar et al. 2019). Notably, the neural oscillations of PV+ neurons also regulate fear memories and associative memories (Yau et al. 2021; Nahar, Delacroix, and Nam 2021).

Depletion of PNNs (both by genetic attenuation of PNNs and by ChABC) was found to enhance recognition memory as well as long-term depression in the perirhinal cortex (Romberg et al. 2013). PNNs are also found to have an interesting relationship with spatial learning. Digestion of hippocampal PNN components via ChABC promotes “re-learning” of a once-trained Morris water maze task (a spatial learning task) (Ruzicka et al. 2022), however degradation of PNNs surrounding grid neurons in the medial entorhinal cortex impaired representation of new environments {Christensen, 2021 #420}. By demonstrating that PNN degradation in different regions affect similar memory process in opposing ways, these studies highlight the possible region-specific functionality of PNNs.

Together, these studies, which examine different brain structures and facets of memory, suggest an interesting relationship between PNNs and memory— that they may enhance the acquisition of memories (via increased synaptic plasticity), but decrease the retention of memories (by fundamentally de-stabilizing synapses).

PNNs in AD brains

The roles of PNNs in regulating synaptic plasticity and transmission as well as memory formation and retention make them logical points of investigation in dementia-causing disorders such as AD. However, the relationship between AD pathogenesis and PNN presence and function remains largely unknown.

Histological studies of human AD brains, as well as mouse models of Aβ and Tau pathologies, have aimed to determine the effect (and/or correlates) of AD pathology on PNN presence in the brain. These studies typically use either WFA antibodies, which recognize the CS-GAG side chains of PNNs, or aggrecan antibodies which recognize the most common CSPG core protein. Likely due to the variations in the antibodies used, the brain regions they examine, and the imaging techniques used, these studies have had varying findings.

In studies of human brain sections, some researchers have found a reduction in PNN CS-GAGs in AD while others report that the levels remain unchanged (Kobayashi, Emson, and Mountjoy 1989; Baig, Wilcock, and Love 2005; Morawski, Pavlica, et al. 2010). Conversely, human studies investigating the core protein CPSGs (using aggrecan antibodies or other members of the lectican family) have reported decreased PNNs, unchanged PNNs, or even increased PNNs in AD (Lendvai et al. 2013; Crapser et al. 2020; Howell et al. 2015; Morawski, Pavlica, et al. 2010; Morawski, Bruckner, et al. 2010).

As in the human studies, investigation of mouse models of AD pathologies have also shown inconsistencies. Specifically, studies investigating WFA+ reactivity (in different brain regions and mouse models) have reported increased (Vegh et al. 2014), decreased (Crapser et al. 2020; Javonillo et al. 2021) and unchanged (Sos et al. 2020) levels of WFA+ PNNs in response to

AD pathology. The divergent findings in these studies point to the heterogeneity of the PNN structure and suggest that PNNs may play an important role in AD pathogenesis in a region-specific manner. Further, the apparent discrepancies across these studies highlight the importance for a comprehensive study that analyzes all critical components of PNNs, in several critical brain regions, across disease timepoints.

Beyond the presence of PNNs, several histological studies have also examined the relationship between PNNs and the individual pathologies of AD. For instance, Morawski et al. and Lendvai et al. found that neurons containing hyperphosphorylated Tau lack PNNs. Morawski et al further posit that aggrecan-based PNNs protect against neuronal vulnerability and may be involved in neuroprotection in AD. Further analyses must be conducted to better understand the relationship between PNNs and the NFTs and Aβ plaques themselves.

Furthermore, recognizing the important relationship between PNNs and PV+ neurons as well as the importance of PNN composition to their function, Yamada et al. characterize the WFA+ and Aggrecan+ reactivity of PV+ neurons in the cornu ammonis (CA) fields of the hippocampus. Similar experiments, gauging PNN composition surrounding PV+ neurons should be replicated in AD models, to better understand the roles of PNNs, PV+ neurons, and the relationship between the two in AD.

Goal of Present Study

To better understand how PNNs and PV+ neurons react and/or contribute to AD pathogenesis, we propose a histological study examining both WFA+ and Aggrecan+ PNNs and PV+ neurons in the anterior cortex, posterior cortex, and within the subiculum at varying time points in the 5XFAD (amyloidosis) mouse model. This study will help resolve inconsistencies in

previous studies and provide a more comprehensive understanding of how AD-type pathology (specifically, amyloidosis) affects regional PNN composition in the mammalian brain. Furthermore, this study will assess how amyloidosis affects regional PNN composition specifically surrounding PV+ neurons. This will provide novel insight into the relationship between AD pathogenesis and regional PV+ neuronal loss as well as how amyloidosis affects the association of PV+ neurons with individual PNN components. The present document serves as the first part in this ongoing study by examining WFA+ PNNs and PV+ neurons in cortical regions and within the subiculum of 3-month, 6-month and 10-month Wild Type (WT) and 5XFAD brains.

Materials and Methods

Subjects

All mice used in the present study were housed in the Department of Animal Resources at Emory University under a 12 h light/12 h dark cycle with ad libitum access to food and water. Animals were housed in the vivarium under standard conditions for mice (temperature 72 F, humidity range 40–50%). All procedures were approved by the Institutional Animal Care and Use Committee of Emory University and were in strict accordance with the National Institute of Health's "Guide for the Care and Use of Laboratory Animals" PROTO201700821.

In this study, we utilize the 5XFAD mouse model, a model organism for AD that expresses mutant APP and PSEN1 transgenes to produce progressive and severe Aβ pathology in the brain (Oblak et al. 2021). Notably, 5XFAD mice exhibit intraneuronal $A\beta_{42}$ around 1.5 months of age and begin developing plaques around 2 months of age. Neuronal death begins around 6 months as plaques continue to accumulate (Eimer and Vassar 2013).

For this study, ~ 8 5XFAD mice and ~8 Wild-Type (WT) mice (which serve as controls) were euthanized via isoflurane at each of the following time points: 1.8 months, 3 months, 6 months, and 10 months (exact number of mice in each group presented in Figure 1). Following euthanasia, mice were perfused using 1X PBS and brain tissue was collected. Brains were fixed using 4% paraformaldehyde and cryoprotected in 30% sucrose and 0.05% sodium azide prior to sectioning. Using a freezing microtome, brains were sectioned into 30 µm sections. Brains were serial sectioned into 24 well places such that each well contained equally representative sections of the entire brain.

Tissue Staining

Sections were removed from cryoprotectant and rinsed with 1X PBS for 10 minutes. Next, the sections were permeabilized using 0.3% triton-X in 1X-PBS. This reagent serves to dissolve lipids on cell membranes such that large antibodies can access intracellular antigens (Chen, Cho, and Yang 2010). Following this step, blocking using 0.3% Triton-X and 1% Bovine Serum Albumin (BSA) was conducted for 2 hours shaking at room temperature to prevent non-specific antibody binding. Brain sections were then treated with the following primary antibodies overnight at 4 degrees C in 0.3% Triton-X and 1% BSA: WFA (an antibody widely used to target CS-GAG components of the perineuronal nets) (Vector Anti-WFA Ref: B-1355 [1:100]), PV (abcam ab181086 [1:200]), and 4G8 (a widely used anti- Aβ monoclonal antibody) (BioLegend Cat: 800701 [1:2,000]).

The following day the sections were rinsed 3 times for 10 minutes each in 0.3% Triton-X to remove residual primary antibody. The sections were then stained with the following secondary antibodies for 1 hour, shaking at room temperature: (Streptavidin Dylight 488 Cat: 21832 [1:1,000]), (ThermoFisher Donkey Anti-Mouse IgG Alexa 555 Cat: A32773 [1:1,000]), and (ThermoFisher Donkey Anti-Rabbit IgG Alexa 694 Cat: A32795 [1:1,000]). Each secondary antibody is conjugated to a fluorophore and selectively recognizes one of the aforementioned primary antibodies. This allows for the visualization of each desired antigen when using immunofluorescent microscopy.

Following incubation of the secondary antibody, the sections were again rinsed 3 times for 10 minutes each in 0.3% Triton-X to remove residual antibodies. The sections were then stained with DAPI (1:1000) for 2 minutes followed by 2, 2-minute rinses of 1X PBS. DAPI is a nearly

universally used fluorescent stain that binds to DNA to allow visualization of nuclei. Finally, each brain section was mounted onto slides in the same orientation such that the resulting images would be comparable. The next day, or once the slides had sufficiently dried, mounting media was applied, and the slides were cover slipped. Slides sit at room temperature for 24 hours to allow mounting media to dry and were then stored at 4 degrees C**.**

Immunostaining Optimization

Thorough troubleshooting was necessary to acquire sufficient staining of each of the aforementioned antigens: WFA (recognizing GAG side chains of PNNs), PV (recognizing PV+ interneurons), and 4G8 (recognizing Aβ plaques). Prior to this project, our lab used anti-PV antibodies derived from mice. However, this antibody was not an option for this study because the antibody we were using to recognize Aβ, 4G8, was derived from mice. When utilizing Immunohistochemistry (IHC) it is not possible to use two primary antibodies derived from the same host species, because the secondary antibodies (usually) work by selectively recognizing the primary antibodies derived from a specific species. Thus, we conducted test stainings using a new anti-PV antibody derived from rabbit (Abcam Cat: ab181086) at a concentration of 1:500. Initially, we thought this staining had worked, but upon further investigation, the signal picked up by the “anti-PV” channel was identical to that of the “anti-4G8” channel. This indicated that the excitation and emission spectra of the secondary antibody used along with the anti-4G8 primary antibody fell within a range such that the fluorescent signal was picked up by both channels (called “crosstalk”). This was rectified by changing the secondary antibody paired with the anti-4G8 primary antibody— one which had an excitation peak of 555 instead of 594.

This resolved the channel crosstalk but highlighted a new issue: now that the crosstalk signal was gone there was no signal in the anti-PV channel. Aiming to rectify this we utilized a heat-mediated antigen retrieval technique. This technique aims to break methylene bridges formed during tissue fixation to expose antigen-binding sites, allowing the antibodies to effectively bind (Yamashita, 2007 #419). For this technique, we mounted brain sections prior to staining and microwaved them for 10 minutes in a 10 mM sodium citrate buffer at a pH of 6.0 (achieved using the addition of HCl). The rest of the protocol was identical except that the steps took place on the already mounted slides (as opposed to in wells).

The introduction of the antigen retrieval step achieved the goal of effectively visualizing PV+ interneurons, but again a new problem arose: with the inclusion of the antigen retrieval step the anti-WFA antibody no longer labeled PNNs. Aiming to rectify this we acquired two new WFA antibodies. Both primary antibodies were biotinylated and could be recognized and visualized by a Streptavidin antibody conjugated to a fluorophore. However, replicating the staining using both antibodies independently, yielded unsuccessful staining of WFA.

Ultimately, by continually modifying the parameters of our staining protocol, we found a staining protocol that worked for our desired antigens—the protocol described above.

Image Acquisition

All images in this study were obtained using the Keyence BZ-X800 fluorescent microscope. We used the DAPI, FITC, TRITC, and Cy5 Keyence filter sets which each contain an excitation filter, an emission filter, and a dichromatic mirror. Using these filters and our chosen antibody combinations, we can visualize DAPI staining (nuclei), WFA staining (GAG component of PNNs), PV staining (PV+ interneurons), and 4G8 (Aβ plaques) on a given section simultaneously.

Exposure parameters for each channel remained consistent across sections such that image quantification would be comparable.

The Keyence stitching tool was used to obtain a single 4X magnification image containing each of the regions of interest (anterior cortex, posterior cortex, and subiculum). Images of each individual channel were obtained as well as a “merged” image which overlays each channel.

Image Processing

In this study we aim to quantify the counts of PV+ neurons and WFA+ PNNs as well as the percentage of WFA+ PNNs which surrounded a PV+ neuron and the percentage of PV+ neurons which were surrounded by a PNN in the 5XFAD mouse model compared to WT. The determination of PV+ neuronal count, localization, and intensity is easily accomplished via ImageJ (NIH) due to their consistent circular morphology, high intensity, and low background signal. Following the isolation of regions of interest, conversion to a 16-bit image, and imposition of an intensity threshold, the software outputs a CSV file containing the locations and intensities of each PV+ neuron.

However, quantification of the PNNs is more challenging due to their highly irregular and non-circular morphologies, as well as vastly inconsistent background signal. One approach to this is similar to that of PV quantification— using ImageJ, remove background, convert to a 16-bit image and set an intensity threshold. However, this approach requires additional extensive manual intervention with ImageJ’s brush tool to draw lines between adjacent PNNs such that the software does not register them as a single blob. Not only is this impractical but the process of drawing these lines and setting these thresholds, introduces substantial subjectivity and

variability into the images (setting of a threshold introduces less subjectivity in the PV images due to their relatively low background).

Interestingly, a January 2023 pre-print by Lupori et al. presents another option for quantifying PNN (and PV) localization: a series of deep convolutional neural networks. Trained on ~670,000 manually annotated PNNs, their models input an image (either PV or PNN) and output a CSV containing localizations as well as "scores" (confidence ratings). Conveniently, the authors published their models to their GitHub page (link here). Once we cloned the GitHub repository onto a laptop, 8-bit images from either the PV channel or the WFA channel could employ a series of deep-learning models to "predict" localization and score of each PV+ neuron or PNN.

To qualitatively determine the accuracy of both the ImageJ approach and the deep-learning networks two short python scripts were created that map the determined localizations onto the original image. This allows us to qualitatively assess the relative false positive and false negative frequencies of both methods.

Furthermore, we varied many parameters (including file type, bit depth, degree of "background removal" and image brightness) to probe the factors which affect the efficacy of the deep-learning models created by Lupori et al. We found (qualitatively) vastly different degrees of effectiveness on our images. We saw more accurate scoring when the PNNs were less dense, when there was less background signal, and when the PNNs were at high resolution.

Due to the lack of consistency seen when using the models developed by Lupori et al., the data shown in this document is acquired using manual annotations of the PNNs in each image.

However, we remain optimistic regarding the possibility of using the resources developed by Lupori et al. to train our own models that will perform better on our images in the future.

Data Integration and Analyses

While multiple techniques to analyze the localization of WFA+ PNNs were considered, we ultimately used the data acquired from the manual annotation of WFA+ PNNs using the ImageJ point tool. The annotation of WFA+ PNNs and PV+ neurons of the 3-month and 6-month brains yielded 256 CSV files — each representing either PV+ neuron or WFA+ PNN localizations within an individual ROI for an individual mouse. To analyze the relationship between genotype (5XFAD or WT) and age (3mo or 6mo) on PV+ neuron and WFA+ PNN counts and their co-localization, the 256 files needed to be integrated into a single data frame. This was accomplished by organizing the files into a specific folder hierarchy and inputting the parent directory into the R script *Processing.R* (Appendix B). This R script integrates the data and creates a data frame in which each row represents one brain, and there are columns for age and genotype, as well as PV+ neuron count, WFA+ PNN count, the percentage of WFA+ PNNs surrounding a PV+ neuron (%PV+ PNNs), and the percentage of PV+ neurons surrounded by a WFA+ PNN (%PNN+PVs) for each of the 3 ROIs. A given PV+ neuron and WFA+ PNN were deemed to colocalize if their center point was less than 10 pixels from each other in both the X and Y directions.

Paired boxplots in Figures 2-7 visualize how PV+ neuron count, PNN count, %PV+ PNNs, and %PNN+ PVs differ based on age and genotype within each ROI. To examine the statistical significance, two-way ANOVA tests are conducted on the data displayed in each boxplot. These analyses assess the effect of age, genotype, and the interaction between age and genotype for

each variable within each ROI. The ANOVA outputs can be found in Appendix A and the findings are discussed below.

Furthermore, while the small sample size of 10-month WT brains (N=2) hindered us from including data from this time point in Figures 2-7, we use an alternative method to assess how the %PV+ PNNs and the %PNN+ PVs changes from 6 months to 10 months in the 5XFAD and WT brains. For this, we develop another R script (*Processing_Plaques.R* found in Appendix B) that inputs the coordinates of WFA+ PNNs and PV+ neurons from the anterior cortex of 1 WT 6 month old mouse, 1 WT 10-month old mouse, 1 5XFAD 10-month old mouse, and 1 5XFAD 6-month old mouse, and conducts two logistic regressions to examine the effect of age and genotype on the likelihood that a given PV+ neuron is surrounded by a PNN or vice versa. These regression analyses as well as bar plots for visual aids are shown in Figures 8-9 and Tables 1-2.

Finally, we aim to quantitatively examine the relationship between the Aβ pathology and the likelihood that a given PV+ neuron is surrounded by a WFA+ PNN and vice versa. To approach this, we aim to understand how the proximity to an Aβ plaque affects either of these variables. To examine this, we used data from 1 6-month-old 5XFAD mouse and 1 10-month-old 5XFAD mouse and conducted a logistic regression to analyze the relationship between proximity to a plaque, size of the nearest plaque, age, interactions between these co-variates, and likelihood for a PV+ neuron to be surrounded by a PNN and vice versa. These analyses were also completed using *Processing_Plaques.R* found in Appendix B. The outputs of these analyses can be found in Table 3 and Table 4. Grouped boxplots and other plots are shown in Figure 10 and Figure 11 to aid in visualizing the relationship between proximity to plaque and probability of colocalization.

Results and Discussion

In this study, we began by examining the effect of age and genotype on the count of PV+ neurons and WFA+ PNNs in the cortex (both anterior and posterior) and in the subiculum. An overall summary of the study workflow is presented in Figure 1. While WT and 5XFAD mice of 1.8, 3, 6, and 10 months of age were sectioned and stained, only the 3 and 6-month old mice were examined in this portion of the study due to time limitations and sample size limitations within the 10-month old cohort. It is thus important to note that in the 5XFAD amyloidosis mouse model used in this study, Aβ plaques have just begun to accumulate at 3 months of age, and at 6 months of age the plaques are ubiquitous and neuronal loss begins (Eimer and Vassar 2013).

The PV+ neuron counts in the anterior cortex, posterior cortex, and subiculum by age (3 vs 6 month) and genotype (5XFAD vs WT) were visualized using grouped boxplots shown in Figures 2B, 4B, and 6B respectively. These plots along with the two-way ANOVA tests found in Appendix A, showed that PV+ neuron counts differ significantly between age groups, but not between genotype groups of the posterior cortex and subiculum. Specifically, PV+ neuron counts in these regions were significantly higher in the 6-month mice compared to the 3-month mice. Within the anterior cortex, PV+ neuron counts did not differ significantly by either age or genotype.

The WFA+ PNN counts within these brain regions were similarly examined. Unlike the PV+ neuron count, WFA+ PNN counts did exhibit genotype-specific changes. In all three regions analyzed, the 5XFAD model exhibited significantly lower counts of WFA+PNNs compared to the WT model. This finding reinforces the hypothesis that amyloidosis affects synaptic connections by causing the degradation of stabilizing PNNs.

Additionally, the WFA+ PNN counts varied by age, with the 6-month brains having higher counts of WFA+ PNNs in both the WT and 5XFAD mice for all three brain regions. The increase in PV+ neurons and WFA+ PNNs from 3 months to 6 months possibly indicates the completion of neurodevelopmental critical periods during this time frame, as an increase in perineuronal nets is known to regulate the closure of critical periods (Carulli and Verhaagen 2021).

Beyond the presence of PV+ neurons and WFA+ PNNs, we aimed to examine how amyloidosis affects the association between them, again in the 3-month and 6-month mice brains. To do this we examined both the percentage of PV+ neurons that were surrounded by a WFA+ PNN (%PNN+PVs) and the percentage of WFA+ PNNs that surrounded a PV+ neuron (%PV+PNNs). A decrease in the percentage of PV+ neurons surrounded by a WFA+ PNN could indicate a depletion of WFA+ PNNs surrounding PV+ neurons, but it is unclear whether WFA+ PNNs are being depleted in a universal manner, or a manner specific to PV+ neurons. Conversely, a decrease in the percentage of WFA+ PNNs surrounding PV+ neurons could indicate the depletion of WFA+ PNNs specifically surrounding PV+ neurons or the increase in WFA+ PNNs surrounding neurons other than PV+ neurons. However, a decrease in both metrics would indicate that WFA+PNNs were being depleted surrounding PV+ neurons in a preferential manner. Thus, examining both metrics is crucial to understanding how the association between PV+ neurons and WFA+ PNNs is altered in reaction to Aβ pathology.

Using two-way ANOVA tests, we found that in the anterior cortex, the posterior cortex, and the subiculum, the 5XFAD mice exhibited significantly lower %PNN+ PVs (Figure 3B, Table B3; Figure 5B, Table B7; Figure 7B, Table B11). The only one of these three regions that exhibited an age-specific change, was the posterior cortex, yielding higher %PNN+ PVs in the 6-month mice.

However, we did find that the interaction between age and %PNN+PVs was significant in both the anterior and posterior cortex. This indicates that the 5XFAD mouse model affects the association of WFA+ PNNs with PV+ neurons in a time-dependent manner. Specifically, the 5XFAD mice exhibited a greater decrease in %PNN+ PVs compared to WT at the 3-month time point compared to the 6-month time point in both the anterior and posterior cortex. This is contrary to the hypothesis that as amyloidosis progresses (here measured in time), the pathology will have a greater effect on the association between PV+ neurons and PNNs compared to controls. Our findings here—that there was a greater effect of the 5XFAD mouse model at 3-months compared to 6-months— could indicate that the presence of the emerging pathology in the 3-month brain greatly affects the regulation of critical periods and their closure known to be regulated by and/or associated with PV+ neurons and PNNs. Further *in-vivo* and *in-vitro* analyses must be conducted to analyze how intracellular Aβ (seen prior to plaque deposition) affects the ability of PV+ neurons and PNNs to regulate critical periods of development.

Further, the finding that the %PNN+ PVs are significantly decreased in the 5XFAD mice at 3-months and 6-months indicates that in the relatively early stages of amyloidosis, WFA+ PNNs around PV+ neurons are degraded, and/or the Aβ pathology hinders the formation of PNNs surrounding PV+ neurons. It is not clear, however, whether the degradation or inability of the formation of WFA+ PNNs is specific to PV+ neurons.

To investigate this last point, we examined the %PV+ PNNs. We found that in all three brain regions, age but not genotype was significantly correlated with %PV+ PNNs, with 6-month mice having significantly higher %PV+ PNNs. (Figure 3C, Table B4; Figure 5C, Table B8; Figure 7C,

Table B12). This suggests that in the 5XFAD brain at 3 and 6 months, WFA degrades (and/or is unable to form) around all classes of interneurons, not selectively on PV+ interneurons.

Furthermore, while we were unable to examine the 10-month old mice alongside the 3-month and 6-month mice due to sample size limitations, we used an alternative approach to investigate how amyloidosis affects the %PNN+ PVs and the %PV+ PNNs at the 10-month time point: we utilized logistic regression models which used age and genotype as predictors to assess whether an individual PV+ neuron is accompanied by a WFA+ PNN or vice versa. For these analyses, we used an N=1 for WT 6-month mice, WT 10-month mice, 5XFAD 6-month mice, and 5XFAD 10-month mice. In these analyses, individual PV+ neurons or WFA+ PNNs were treated as a sample as opposed to individual mice in the previous analyses. However, because only one mouse from each group was examined, the results of these analyses are preliminary and require further investigation to be confirmed. Notably, these analyses only examine the anterior cortex. The first of these analyses found that the probability of a PV+ neuron being associated with a WFA+ PNN is significantly correlated with both age and genotype. The older mouse (10-month compared to 6-month) had a significantly lower %PNN+ PVs. Similar to the data observed when comparing the 3-month and 6-month mice, the 5XFAD mice had a lower %PNN+ PVs. This suggests that amyloidosis caused a loss of WFA+ PNNs surrounding PV+ neurons (whether it be specific to PV+ neurons or not). Notably, the interaction between age at genotype was not significant for either of these findings, indicating that the effect of amyloidosis did not differ by age (Figure 8, Table 1).

Furthermore, a logistic regression model that used age and genotype to predict whether a given WFA+ PNN surrounds a PV+ neuron found that genotype, but not age, was a significant

predictor of PV+ neuron association. In this model, WFA+ PNNs in 5XFAD mice were significantly less likely to be associated with a PV+ neuron (Figure 9, Table 2). Together, the findings from the first logistic regression (that PV+ neurons were less likely to be associated with WFA+ PNNs in the 5XFAD mouse) and the second regression (that WFA+ PNNs were less likely to be associated with the PV+ neurons in the 5XFAD mouse) collectively indicate that in later stages of amyloidosis, WFA+ PNNs degrade selectively surrounding PV+ neurons.

At face value, these finding differ from those found when comparing the 3-month and 6-month mice. In those mice, genotype did not significantly correlate with %PV+ PNNs. Because of this, we were not able to assert that PNNs degrade specifically around PV+ neurons, but rather that PNNs were likely degraded regardless of the classes of neurons they surrounded. This difference suggests that the association of WFA+ PNNs with PV+ neurons is affected in the 5XFAD mouse in a time-dependent manner. Specifically, WFA+ PNN depletion is exhibited in the 5XFAD mouse brain between 3-6 months, but this depletion is not specifically surrounding PV+ neurons. Then, between 6-10 months the depletion of PNNs occurs in a selective manner around PV+ neurons. Future analyses should perform comprehensive comparisons across time points simultaneously, an approach that was impossible in the present study due to sample size limitations.

Finally, we aimed to assess whether the proximity to an Aβ plaque affects the likelihood of a WFA+ PNN being associated with a PV+ neuron or vice versa. These analyses show that the probability of a PV+ neuron being associated with a WFA+ PNN does not depend on its proximity to an Aβ plaque (or the size of the nearest Aβ plaque) (Figure 10, Table 3). However, the probability of a WFA+ PNN being associated with a PV+ neuron, does significantly correlate with

proximity to an Aβ plaque. Interestingly, this is a significant negative relationship indicating that the closer a WFA+ PNN is to an Aβ plaque, the more likely it is to be surrounding a PV+ neuron. This unexpected finding could imply that WFA+ PNNs surrounding PV+ neurons near Aβ plaques are less vulnerable to degradation than WFA+ PNNs surrounding PV- neurons.

This latter result appears somewhat contradictory to our finding that WFA+ PNNs are selectively degraded in the later time points in the 5XFAD mouse model. Together these findings may suggest that at the 6 and 10-month time points WFA+ PNNs are selectively degraded surrounded PV+ neurons in the anterior cortex; however, in close proximity to Aβ plaques, WFA+ PNNs are selectively protective of PV+ neurons. Alternatively, these findings could result if the density of PV+PNNs coincidentally co-localizes with regions of high Aβ plaque load. Future experiments should assess this by examining regions of high Aβ plaque load and determining the regions of high WFA+ PNN association with PV+ neurons in WT brains. Significant co-localization between these regions could pose an alternate explanation for the data observed in this study.

Interestingly, throughout this study we saw similar findings across the three brain regions analyzed. We intentionally examined large cortical regions to understand how our variables of interest were affected in the cortex as a whole, and to reduce bias that comes with selecting small regions of interest. While this approach helped make the results in this study particularly interesting, these findings should not be misunderstood to suggest that Aβ amyloidosis affects PV+ neurons, WFA+ PNNs, and their association in the same manner across cortical regions. Future research should aim to simultaneously examine several cortical sub-regions (in a methodical manner to reduce bias) in order to understand the region-specific effects of Aβ amyloidosis.

Limitations

In this study, we investigate how PV+ neurons, WFA+ PNNs, and the association between them are altered in AD-type pathology using the 5XFAD mouse model. While mice of 1.8, 3, 6, and 10 months were sectioned and stained, only 3-month and 6-month brains are included in most analyses in this paper due to time limitations and sample size limitations. Thus, the scope of much of our analyses was limited to early amyloidosis.

Further, the method of analyzing %PNN+ PVs and %PV+ PNNs differed significantly from the 3 and 6-month month comparison to the 6 and 10-month comparison, again due to the sample size limitation. Due to the difference in statistical approach, it may not be appropriate to compare the results of these two analyses.

Also, the only antibody used to investigate PNNs in this study was WFA which selectively recognizes the GAG side chains of PNNs. Thus, the findings here pertaining to WFA+ PNNs may not represent the comprehensive changes of the PNNs as a whole in reaction to amyloidosis.

Future Directions

Much of this study investigates the effects of amyloidosis at 3-months and 6-months of age, time points prior to significant neuronal loss in the 5XFAD mouse model. Thus, we plan to acquire a larger sample size of 10-month and 18-month WT and 5XFAD mice and repeat these analyses to better understand how severe Aβ amyloidosis affects PV+ neurons, PNNs, and the association between them.

Furthermore, we plan to replicate this study (across a wider range of age points) using antibodies against CSPG core proteins (aggrecan, brevican, neurocan, etc.) to expand the biochemical scope related to PNN heterogeneity. Using these approaches, we can understand

how the composition of PNNs change in reaction to amyloidosis and whether this change is specific to PNNs surrounding PV+ neurons.

Conclusions

This study shows that WFA+ PNNs, but not PV+ neurons were significantly diminished in the anterior cortex, posterior cortex, and subiculum of 5XFAD mouse brains at 3 and 6 months of age. Further, by analyzing the co-localization between WFA+ PNNs and PV+ neurons, our data suggest that at 3 and 6 month time points the WFA+ PNNs are depleted surrounding PV+ neurons, however in a likely non-exclusive manner. Further preliminary analysis using logistic regression models to compare 6 and 10 month brains suggested that in later stages of Aβ amyloidosis, WFA+ PNNs surrounding PV+ neurons were preferentially depleted. Finally, analyses examining the effect of proximity to Aβ plaques on the association between WFA+ PNNs and PV+ neurons revealed that WFA+ PNNs at a closer proximity to Aβ plaques are more likely to be associated with a PV+ neuron—possibly indicating that PV- neurons are more vulnerable to degradation of WFA+ PNNs by Aβ plaques. Future studies must be conducted to assess how PNNs and their association with PV+ neurons are altered in Aβ amyloidosis, including examining a wider age range as well as multiple critical components of PNN structure.

Figures and Tables

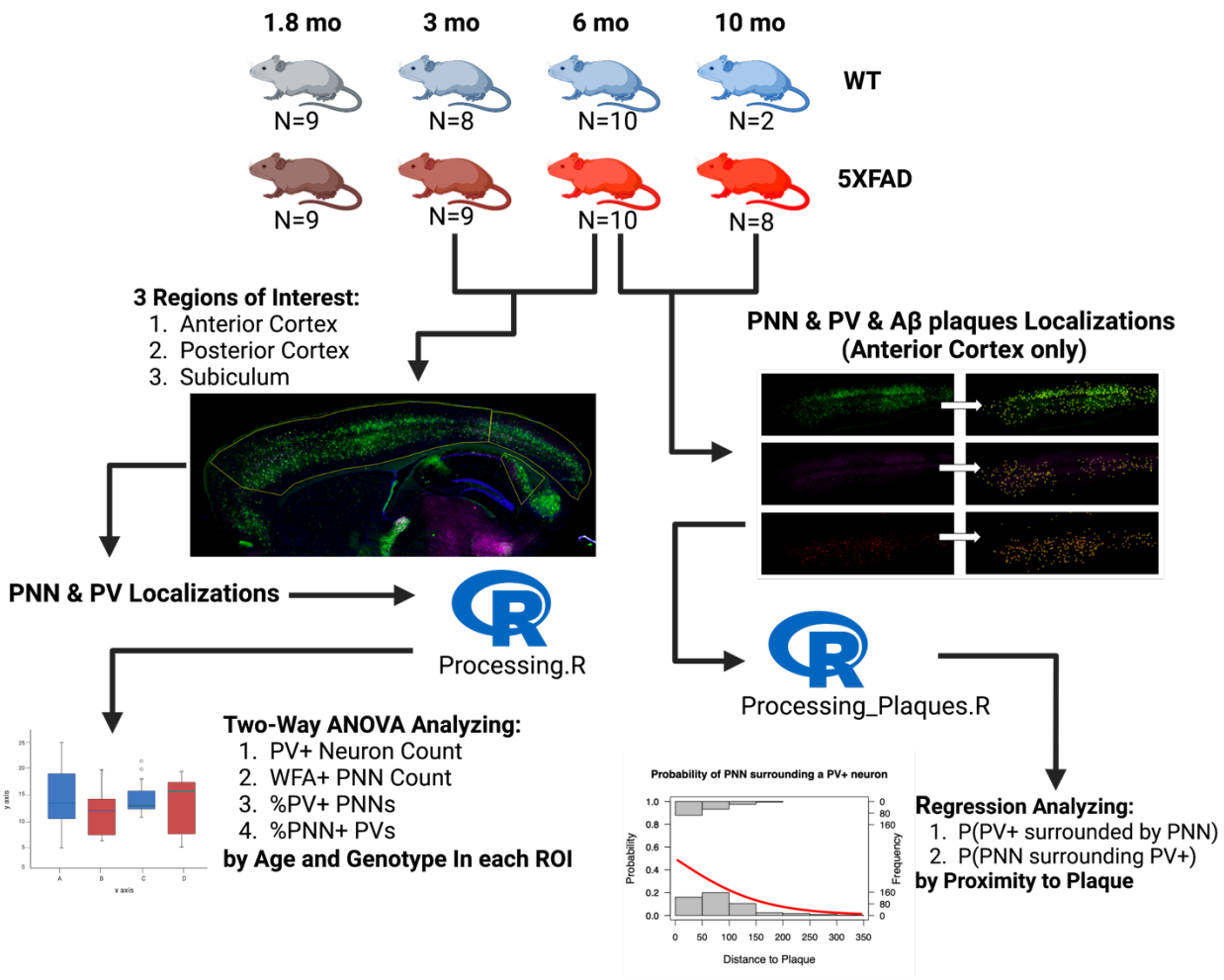

Figure 1. Study Workflow. This study utilizes WT and 5XFAD mice at time points of 1.8, 3, 6, and 10 months. Due to sample size limitations of the 10-month 5XFAD mice and time limitations most analyses were conducted using 3-month and 6-month mice. Three regions of interest were manually determined for each mouse: anterior cortex, posterior cortex, and subiculum. WFA+ PNN and PV+ neuron localizations were determined for each ROI. Data was processed and analyzed through Processing.R (Appendix B). The resulting figures and analyses can be found in Figures 2-7. Further, PV+ neuron, WFA+ PNNs, and Aβ plaque localizations were determined for the anterior cortex of 6-month and 10-month mice. This data was processed using Processing_Plaques.R (Appendix B) and the relationship between plaque proximity and the probability that a given PV+ neuron was surrounded by a WFA+ PNN and verse versa was examined. The resulting figures and analyses can be found in Figures 8-11. (Figure made on BioRender).

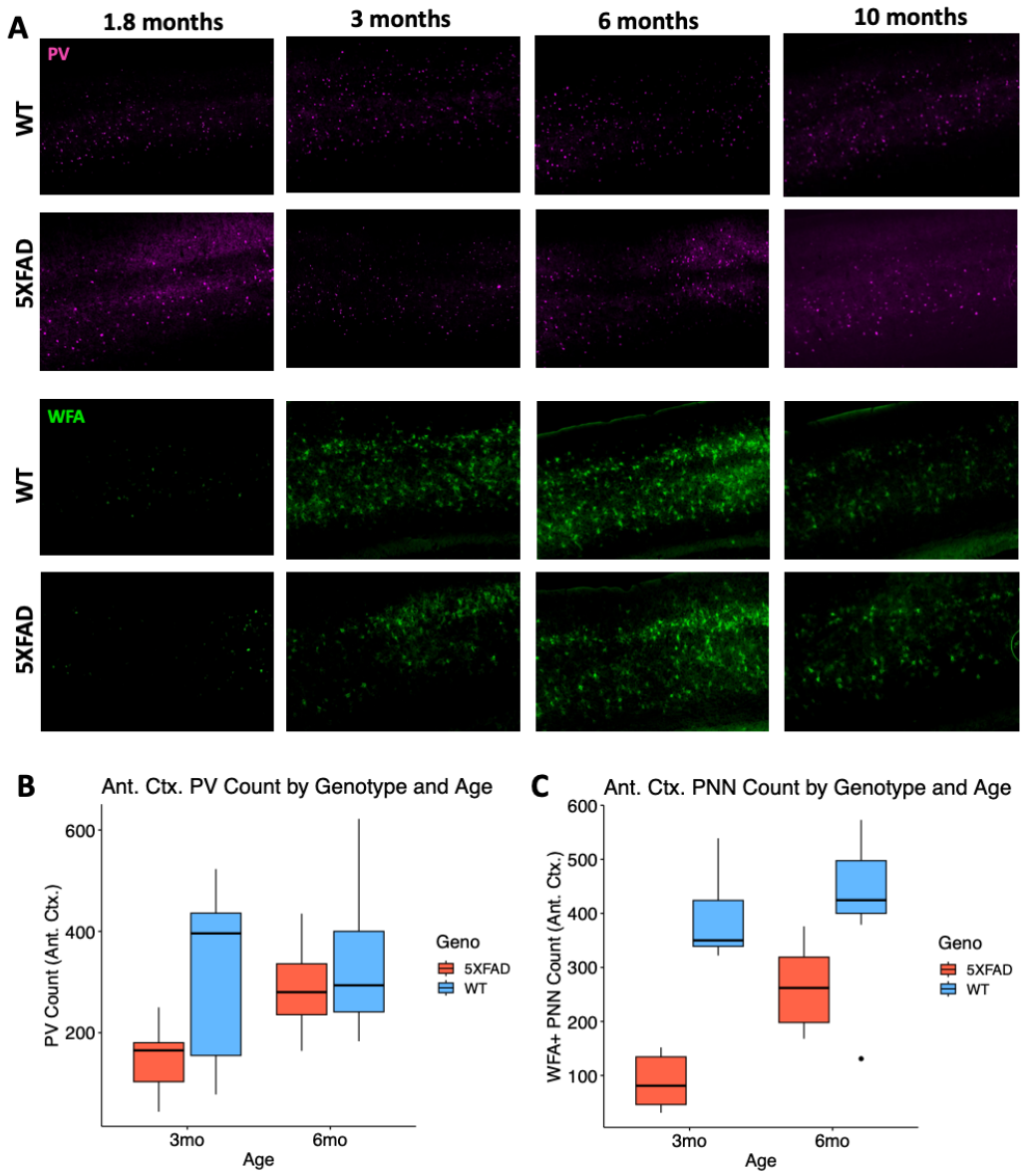

Figure 2. PV+ Neuron and WFA+ PNN Counts in the Anterior Cortex. (A) IHC imaging shows the PV+ neurons (top) and the WFA+ PNNs (bottom) in the anterior cortex of WT and 5XFAD mice at 1.8, 3, 6, and 10 months. Side-by-side boxplots show **(B)** the PV+ neurons count and **(C)** the WFA+ PNN count in the anterior cortex by age (3 months vs 6-month) and genotype (WT vs 5XFAD). Two-way ANOVA output in Table B1 shows that PV+ neuron counts in the anterior cortex do not significantly differ by age or genotype. The two-way ANOVA output in Table B2 shows that WFA+ PNN count in the anterior cortex differs significantly by both age and genotype, although the interaction term is not significant.

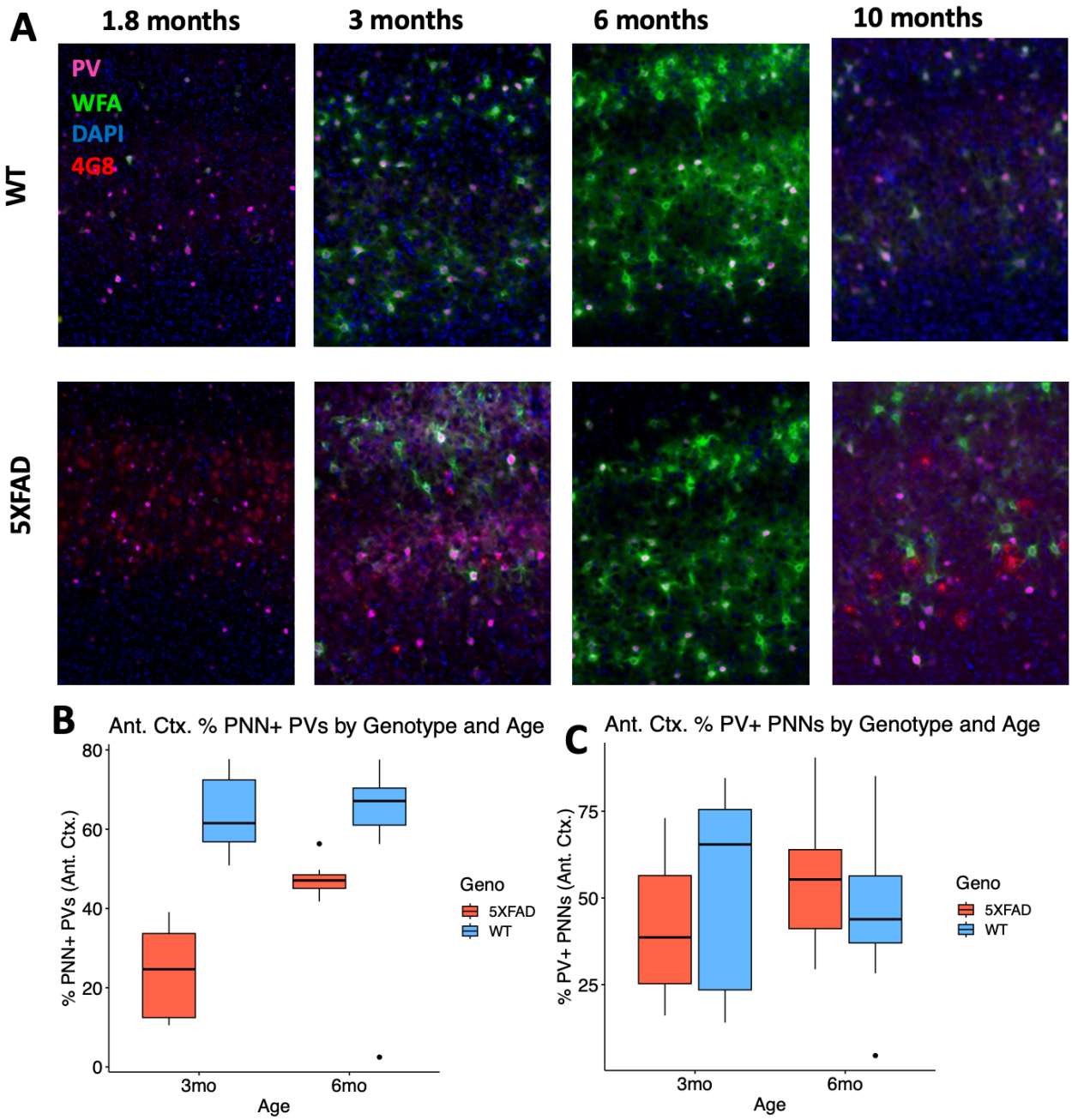

Figure 3. %PNN+ PVs and %PV+ PNNs in the Anterior Cortex. (A) IHC images of the merged WFA, PV, 4G8, and DAPI channels in the anterior cortex of WT and 5XFAD mice at ages 1.8, 3, 6, and 10 months. Side-by-side box plots show **(B)** the % PV neurons surrounded by a PNN and **(C)** the % PNNs that surround a PV+ neuron by genotype (WT vs 5XFAD) and age (3-month vs 6-month). Two-way ANOVA output in Table B3 shows that the %PNN+ PV differs significantly by genotype, and further than this effect is dependent on age (the interaction term is significant). Two-way ANOVA output in Table B4 shows that %PV+ PNNs does not significantly differ by age or genotype.

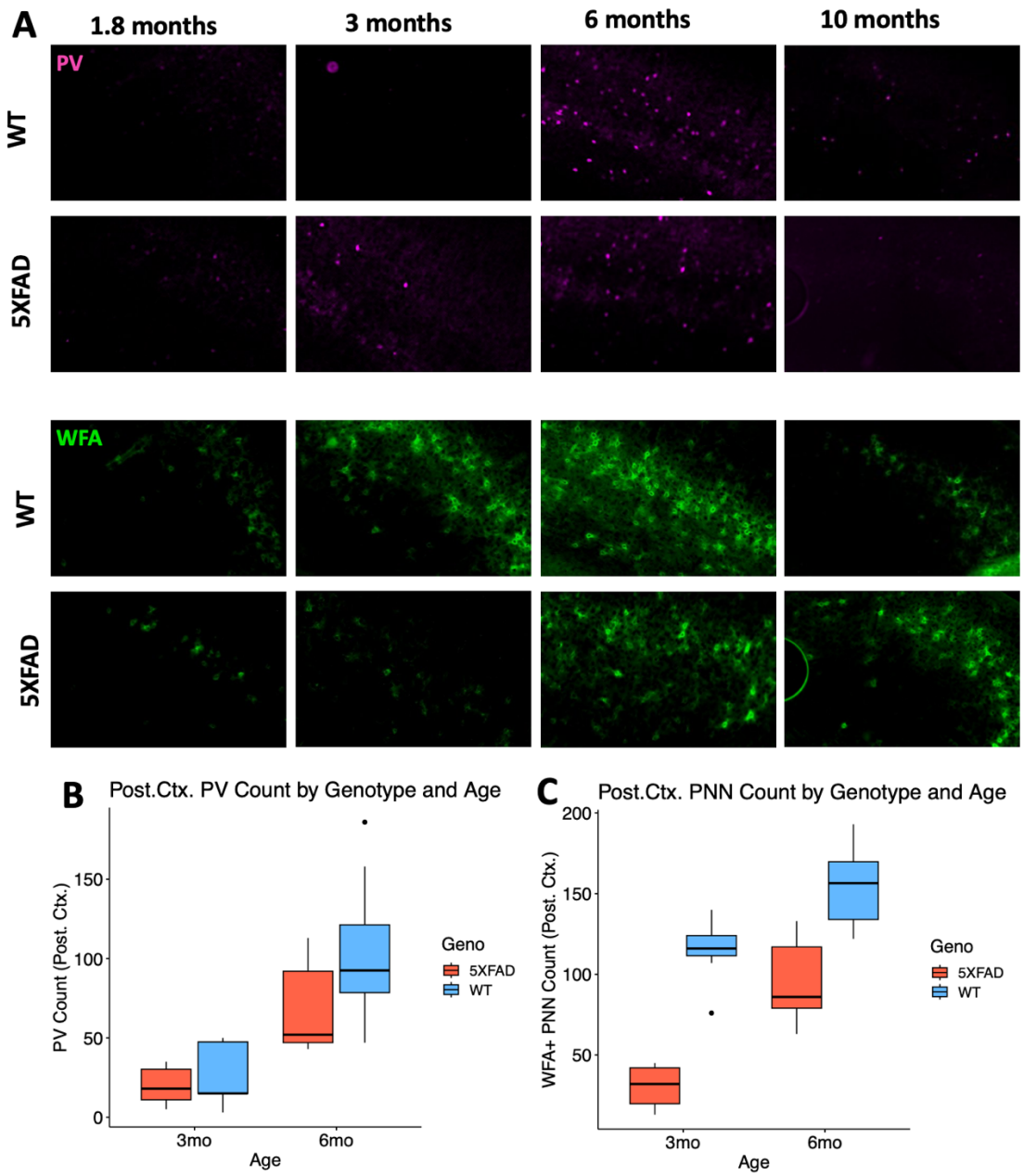

Figure 4. PV+ Neuron and WFA+ PNN Counts in the Posterior Cortex. (A) IHC imaging shows the PV+ neurons and the WFA+ PNNs in the posterior cortex of WT and 5XFAD mice at 1.8, 3, 6, and 10 months. Side-by-side boxplots show **(B)** the PV+ neurons count and **(C)** the WFA+ PNN count in the posterior cortex by age (3 months vs 6-month) and genotype (WT vs 5XFAD). Two-way ANOVA output in Table B5 shows that PV counts in the posterior cortex differ significantly by Age but not by genotype. Two-way ANOVA output in Table B6 shows that WFA+ PNN counts in the posterior cortex differ significantly by both age and genotype.

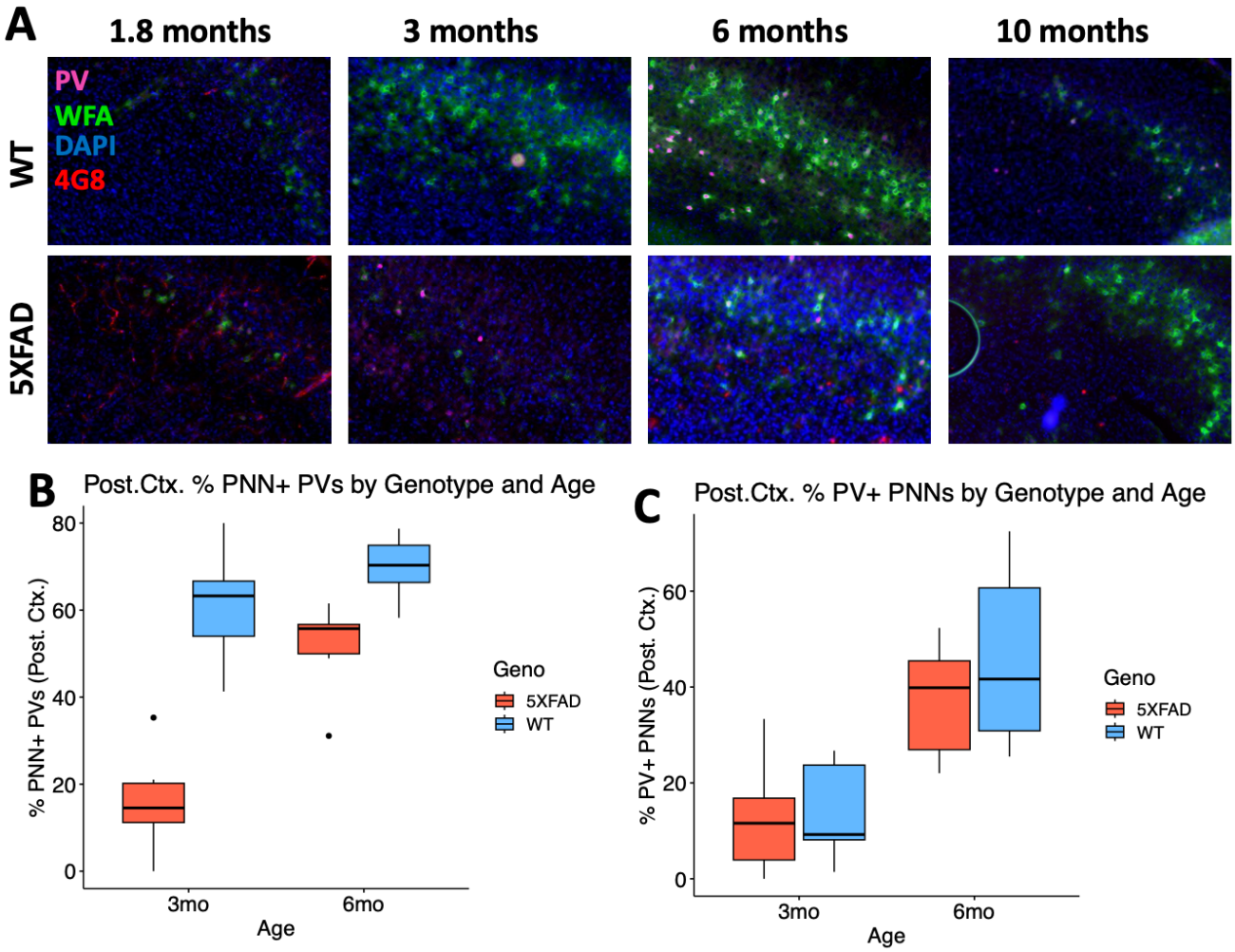

Figure 5. %PNN+ PVs and %PV+ PNNs in the Posterior Cortex. (A) IHC images of the merged WFA, PV, 4G8, and DAPI channels in the posterior cortex of WT and 5XFAD mice at ages 1.8, 3, 6, and 10 months. Side-by-side box plots show **(B)** the % of PV+ neurons surrounded by a PNN and **(C)** the % of PNNs that surround a PV+ neuron by genotype and age (3-month vs 6-month). Two-way ANOVA output in Table B7 shows that the %PNN+ PV differ significantly by genotype and age and further that effect of genotype on %PNN+ PV differ based on age (significant interaction term). Two-way ANOVA output in Table B8 shows that %PV+ PNN in the posterior cortex differs significantly by age, but not genotype.

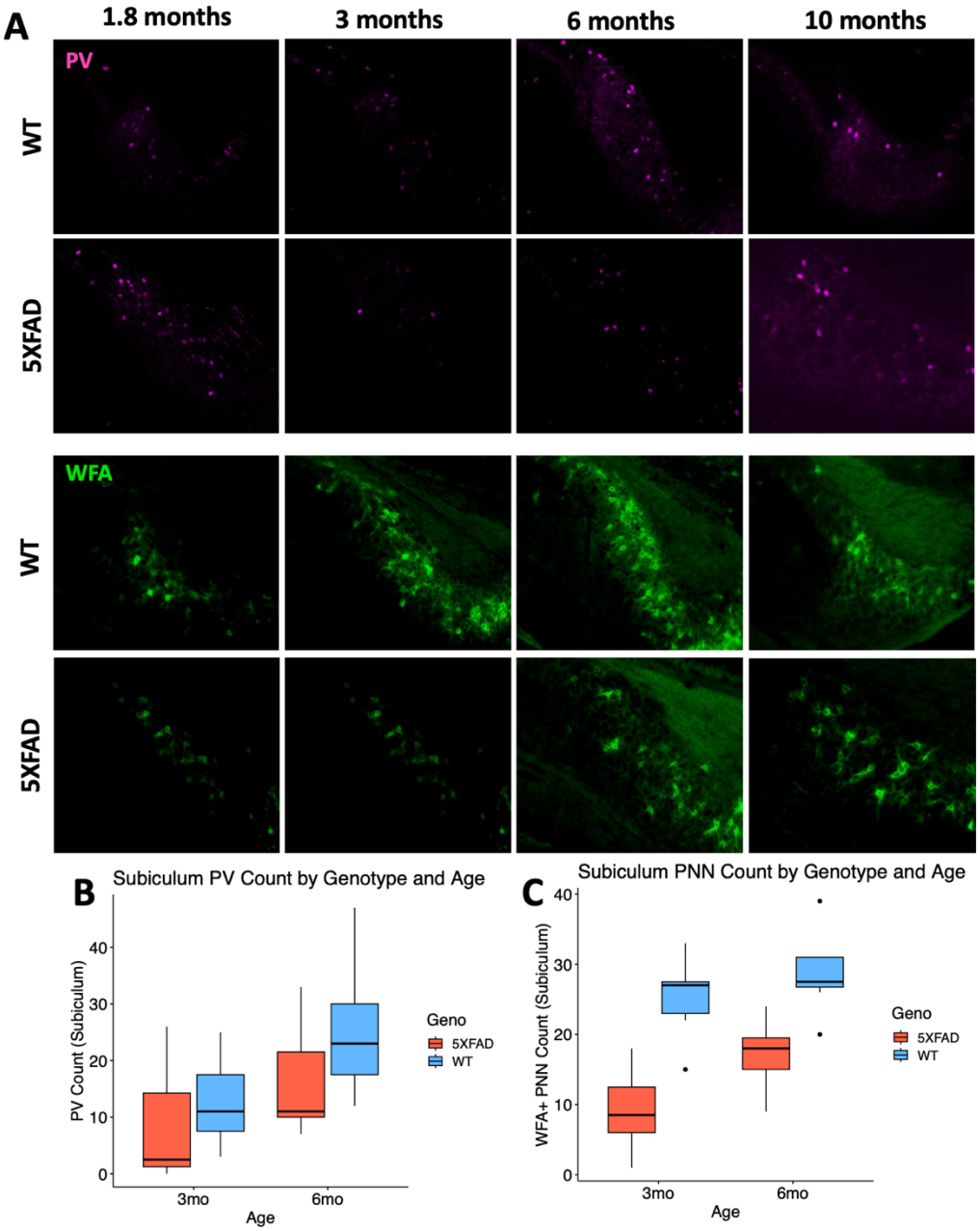

Figure 6. PV+ Neuron and WFA+ PNN Counts in the Subiculum. (A) IHC imaging shows the PV+ neurons and the WFA+ PNNs in the subiculum of WT and 5XFAD mice at 1.8, 3, 6, and 10 months. Side-by-side boxplots show **(B)** the PV+ interneurons count and **(C)** the WFA+ PNN count in the Subiculum by age (3 months vs 6-month) and genotype (WT vs 5XFAD). Two-way ANOVA output in Table B9 shows that PV+ neuron counts in the Subiculum differ significantly by age but not by genotype and ANOVA output in Table B10 shows that PNN counts in the Subiculum Differ significantly by both age and genotype.

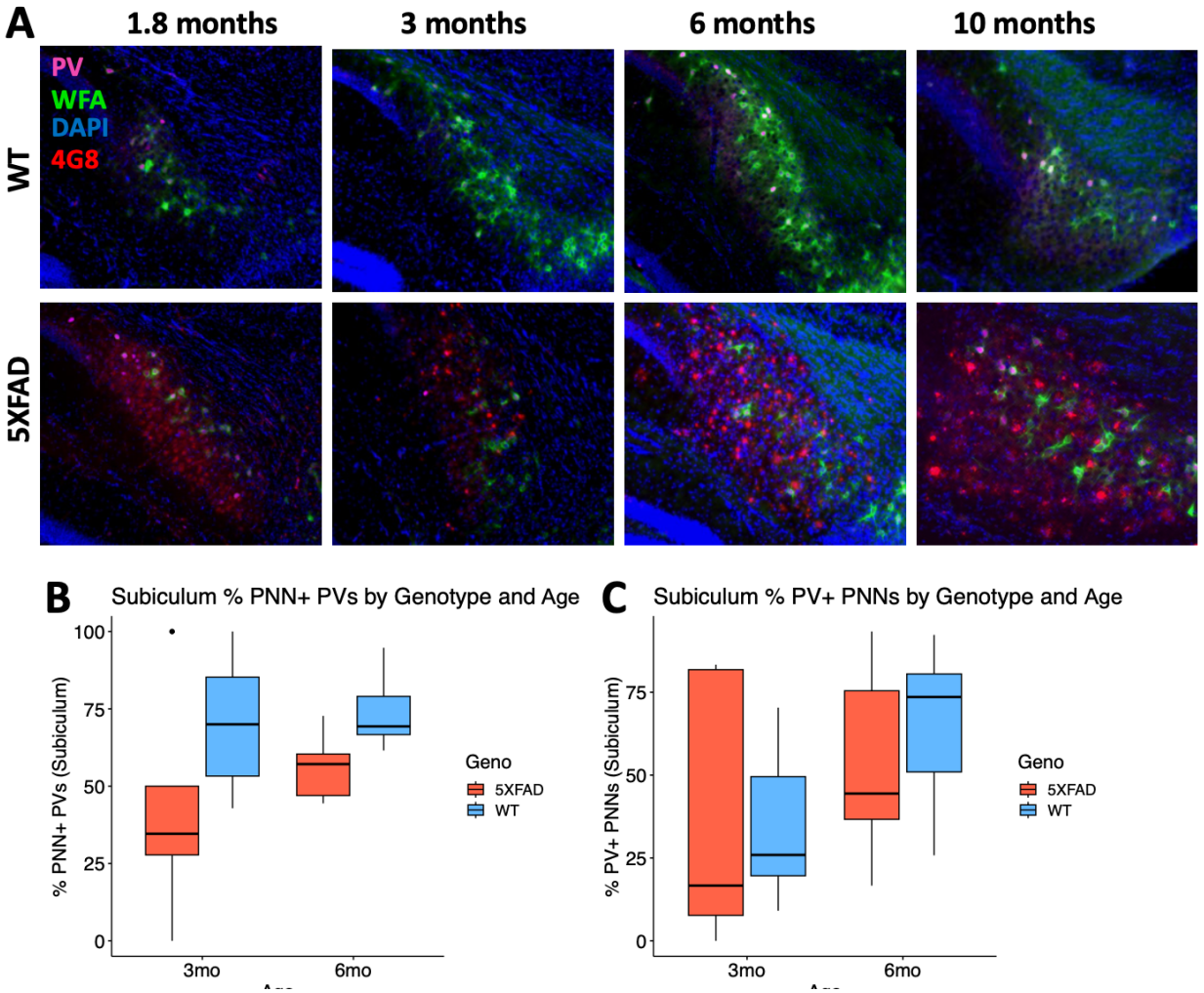

Figure 7. %PNN+ PVs and %PV+ PNNs in the Subiculum. (A) IHC images of the merged WFA, PV, 4G8, and DAPI channels in the subiculum of WT and 5XFAD mice at ages 1.8, 3, 6, and 10 months. Side-by-side box plots show **(B)** the % of PV+ neurons surrounded by a PNN and **(C)** the % of PNNs that surround a PV+ neuron by genotype and age (3-month vs 6-month). Two-way ANOVA output in Table B11 shows that the %PNN+ PVs differ significantly by genotype, but not age. Two-way ANOVA output in Table B12 shows that %PV+ PNNs in the subiculum differ significantly by age, but not genotype.

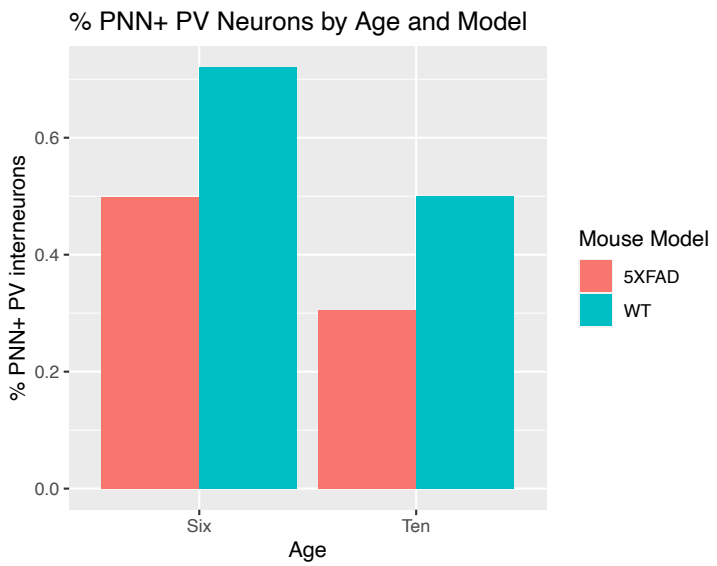

Figure 8. %PNN+ PVs by Age and Genotype in 6 and 10-month mice. % of PV+ neurons surrounded by a WFA+ PNN by age (6-month vs 10-month) and genotype (WT vs 5XFAD). Table 1 below shows the output of a logistic regression model, assessing the significance of the relationships observed in this bar plot.

	Estimate	**Std. Error**	**z value**	**Pr(>|z|)**
(Intercept)	-0.009132	0.135149	-0.068	0.946
Age (10 Months)	-0.814468	0.20458	-3.981	6.86E-05
Genotype (WT)	0.957932	0.174149	5.501	3.78E-08
Age(10): Geno(WT)	-0.134332	0.300465	-0.447	0.655

Table 1. Logistic Regression for Age and Genotype on the Probability that a PV+ Neuron is Surrounded by WFA+ PNN. Logistic regression output assessing if the likelihood that a PV+ neuron is surrounded by a WFA+ PNN differs significantly by age and genotype. This table indicates that there is a significant relationship between both age and genotype on the likelihood that a PV+ neuron is surrounded by a WFA+ PNN.

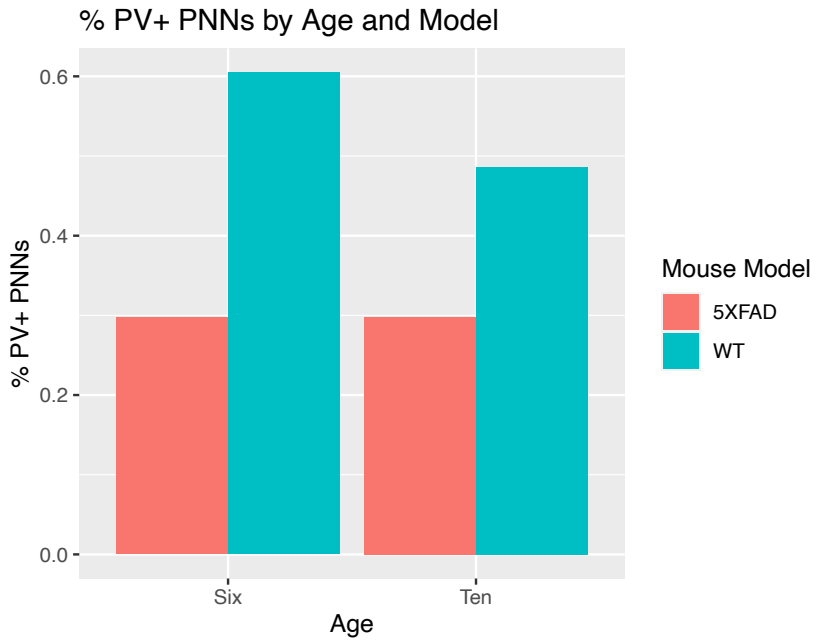

Figure 9. %PV+ PNNs by Age and Genotype in 6 and 10-month mice. % of PNNs surrounding a PV+ neuron by Age (6-month vs 10-month) and Genotype (WT vs 5XFAD). Table 2 below shows the output of a logistic regression model, assessing the significance of the relationships observed in this bar plot.

	Estimate	**Std. Error**	**z value**	**Pr(>|z|)**
(Intercept)	-0.860201	0.113741	-7.563	3.94E-14
Age (10 Months)	0.003729	0.189514	0.02	0.9843
Genotype (WT)	1.285869	0.146193	8.796	< 2e-16
Age(10): Geno(WT)	-0.484457	0.284738	-1.701	0.0889

Table 2. Logistic Regression for Age and Genotype on the Probability that a WFA+ PNN Surrounds a PV+ Neuron. Logistic regression output assessing if the likelihood for a PNN to surround a PV+ neuron differs significantly by age and genotype. This table indicates that there is a significant relationship between genotype, but not age, and the likelihood for a PNN to be surrounding a PV+ neuron.

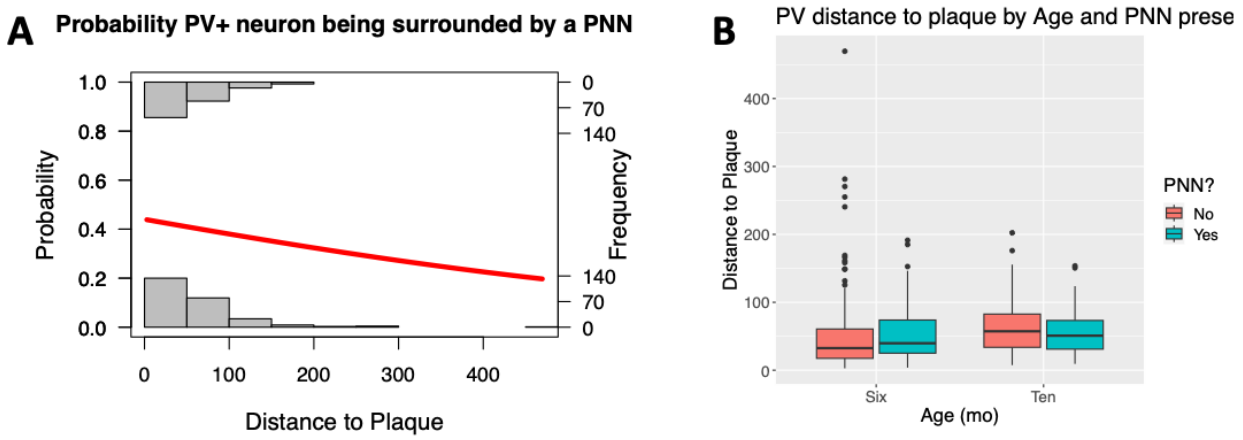

Figure 10. Proximity to Plaque and Probability that PV+ Neuron is Associated with a PNN. These figures visualize the relationship between PV+ neuron proximity to plaque and the likelihood of a PV+ neuron being surrounded by a PNN. **(A)** A plot generated using the logi.hist.plot() function in the popbio R package visualizes the logistic regression of a PV+ neuron proximity to plaque against the probability that a given PV+ neuron is surrounded by a PNN. The histograms on the top and bottom of the plot show the distribution of plaque proximity for PNN- PV+ neurons (bottom) and PNN+ PV+ neurons (top). The red line represents the probability that the PV+ neuron is associated with a PNN as predicted by the model. **(B)** Adjacent boxplots visualize the distance of a given PV+ neuron from a plaque by Age (6-month vs 10 month) and PNN presence. The output of a logistic regression model examining plaque distance, plaque size, and age as predictors for PNN presence around a PV+ neuron is found below in Table 3.

	Estimate	**Std. Error**	**z value**	**Pr(>|z|)**
(Intercept)	3.49E-01	2.68E-01	1.301	0.193
Plaque Distance	-2.29E-03	3.38E-03	-0.677	0.498
Plaque Size	-2.49E-03	1.60E-03	-1.557	0.119
Age (10 months)	-8.54E-01	4.49E-01	-1.904	0.057
PlaqDist:PlaqueSize	6.41E-06	1.56E-05	0.41	0.682
PlaqDist:Age(10)	-3.07E-03	5.48E-03	-0.56	0.576
PlaqueSize:Age(10)	2.11E-03	1.64E-03	1.281	0.2

Table 3. Logistic Regression for Plaque Proximity on Probability that PV+ Neuron is associated with a PNN. The table above shows the output of the logistic regression of Plaque Distance, Plaque Size, Age (6 vs 10 months), and all interaction terms, to predict whether a PV+ interneuron is surrounded by a PNN. The p-values indicate that none of the independent variables, or their interactions, effectively predict PNN presence surrounding PV+ neurons.

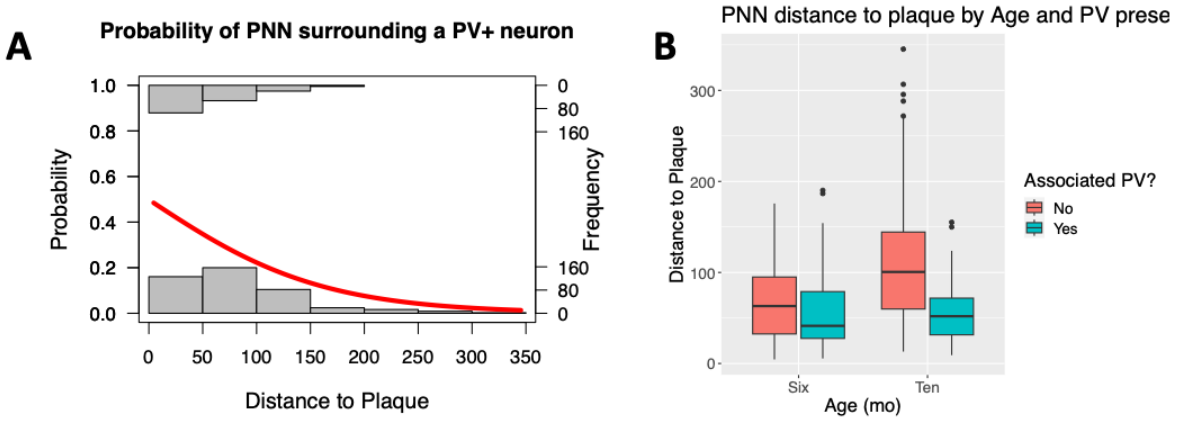

Figure 11. Proximity to Plaque and Probability that WFA+ PNN is Associated with a PV+ Neuron. These plots visualize the relationship between WFA+ PNN proximity to plaques and the likelihood that a given PNN surrounds a PV+ neuron. **(A)** A plot generated using the logi.hist.plot() function in the popbio R package visualizes the logistic regression of WFA+ PNN proximity to plaques against the probability that a given PNN surrounds a PV+ neuron. The histograms on the top and bottom of the plot show the distribution of plaque proximity for PV- PNNs (bottom) and PV+ PNNs(top). The red line represents the probability that the PNN is associated with a PV+ neuron as predicted by the model. **(B)** Adjacent boxplots visualize the distance of a given PNN from a plaque by age (6-month vs 10 month) and PV presence. The output of a logistic regression model examining plaque distance, plaque size, and age as predictors for PV+ association with a given PNN is found below in Table 4.

	Estimate	**Std. Error**	**z value**	**Pr(>|z|)**
(Intercept)	-3.83E-01	2.76E-01	-1.389	0.164758
Plaque Distance	-9.81E-03	3.44E-03	-2.852	0.00434
Plaque Size	-3.36E-04	1.83E-03	-0.183	0.854478
Age (10 months)	1.96E+00	5.22E-01	3.753	0.000174
PlaqDist:PlaqueSize	2.71E-05	1.62E-05	1.676	0.093729
PlaqDist:Age(10)	-1.98E-02	6.21E-03	-3.186	0.001442
PlaqueSize:Age(10)	-2.03E-03	1.75E-03	-1.162	0.245394

Table 4. Logistic Regression for Plaque Proximity on Probability that WFA+ PNN is associated with a PV+ Neuron. The table above shows the output of the logistic regression of plaque distance, plaque size, age (6 vs 10 months), and all interaction terms, to predict whether a PNN is associated with a PV+ neuron. The p-values indicate that Plaque distance, Age, as well as the interaction between them significantly predict whether a given PNN is associated with a PV+ neuron.

Appendix

Appendix A: ANOVA Outputs for Figures 2-7

	Df	Sum Sq	Mean Sq	F value	Pr(>F)
Age	1	52031	52031	2.638	0.1174
Genotype	1	83388	83388	4.228	0.0508
Age:Genotype	1	17053	17053	0.865	0.3617
Residuals	24	473341	19723		

Table B1. ANOVA output Corresponding to Figure 2B. The table above shows the output of the two-way ANOVA test which examines the effect of age and genotype on PV+ neuron count in the anterior cortex. The table shows that at α = 0.05 the difference in PV+ neuron count observed in the boxplot (Figure 1B) do not differ in a statistically significant manner by either age or genotype.

	Df	Sum Sq	Mean Sq	F value	Pr(>F)
Age	1	61107	61107	6.782	0.0156
Genotype	1	346187	346187	38.422	2.10E-06
Age:Genotype	1	37970	37970	4.214	0.0511
Residuals	24	216245	9010		

Table A2. ANOVA output Corresponding to Figure 2C. The table above shows the output of the two-way ANOVA test which examines the effect of age and genotype on WFA+ PNN count in the anterior cortex. The table shows that at α = 0.05 the number of WFA+ PNNs in the anterior cortex differs significantly by Age and Genotype. The interaction term is (barely) non-significant indicating that the effect of both covariates does not depend on the other.

	Df	Sum Sq	Mean Sq	F value	Pr(>F)
Age	1	417	417	1.669	0.208648
Genotype	1	4784	4784	19.138	0.000204
Age:Genotype	1	1269	1269	5.075	0.033684
Residuals	24	5999	250		

Table A3. ANOVA output Corresponding to Figure 3B. The table above shows the output of the two-way ANOVA test which examines the effect of age and genotype on % PV+ neurons associated with a PNN. The table shows that at α = 0.05, WT brains have a significantly higher % of PV+ neurons surrounded by WFA+ PNNs. Further, the interaction term between age and genotype is significant, indicating that the effect of genotype is dependent on age.

	Df	Sum Sq	Mean Sq	F value	Pr(>F)
Age	1	91	91.1	0.144	0.708
Genotype	1	1	0.6	0.001	0.976
Age:Genotype	1	582	582.3	0.919	0.347
Residuals	24	15210	633.7		

Table A4. ANOVA output Corresponding to Figure 3C. The table above shows the output of the two-way ANOVA test which examines the effect of age and genotype on % WFA+ PNN associated with a PV+ neuron. The table shows that at α = 0.05, %PV+ PNNs does not differ significantly by Age or Genotype.

	Df	Sum Sq	Mean Sq	F value	Pr(>F)
Age	1	27876	27876	27.379	2.31E-05
Genotype	1	3225	3225	3.168	0.0878
Age:Genotype	1	1145	1145	1.124	0.2995
Residuals	24	24435	1018		

Table A5. ANOVA output Corresponding to Figure 4B. The table above shows the output of the two-way ANOVA test which examines the effect of age and genotype on PV count in the posterior cortex. The table shows that at α = 0.05 the difference in PV count differs significantly by age, but not genotype.

	Df	Sum Sq	Mean Sq	F value	Pr(>F)
Age	1	18606	18606	38.103	2.23E-06
Genotype	1	34591	34591	70.839	1.27E-08
Age:Genotype	1	1137	1137	2.329	0.14
Residuals	24	11719	488		

Table A6. ANOVA output Corresponding to Figure 4C The table above shows the output of the two-way ANOVA test which examines the effect of age and genotype on PNN count in the posterior cortex. The table shows that at α = 0.05 the number of WFA+ PNNs in the posterior cortex differs significantly by age and genotype.

	Df	Sum Sq	Mean Sq	F value	Pr(>F)
Age	1	3454	3454	29.97	1.26E-05
Genotype	1	6407	6407	55.6	1.07E-07
Age:Genotype	1	1208	1208	10.48	0.00351
Residuals	24	2765	115		

Table A7. ANOVA output Corresponding to Figure 5B. The table above shows the output of the two-way ANOVA test that examines the effect of age and genotype on % PV+ neurons associated with a PNN in the posterior cortex. The table shows that at α = 0.05, the % of PV+ interneurons associated with a PNN in the posterior cortex differs significantly by age and genotype, and further that the respective effects differ based on the state of the other variable (significant interaction effect).

	Df	Sum Sq	Mean Sq	F value	Pr(>F)
Age	1	5462	5462	28.461	1.78E-05
Genotype	1	209	209	1.088	0.307
Age:Genotype	1	86	86	0.448	0.51
Residuals	24	4606	192		

Table A8. ANOVA output Corresponding to Figure 5C. The table above shows the output of the two-way ANOVA test that examines the effect of age and genotype on % PNNs associated with a PV+ neuron in the posterior cortex. The table shows that at α = 0.05, the % of PNNs associated with a PV+ neuron in the posterior cortex differs significantly by age, but not by genotype.

	Df	Sum Sq	Mean Sq	F value	Pr(>F)
Age	1	720.9	720.9	7.105	0.0135
Genotype	1	306.8	306.8	3.023	0.0949
Age:Genotype	1	30.7	30.7	0.302	0.5875
Residuals	24	2435.1	101.5		

Table A9. ANOVA output Corresponding to Figure 6B. The table above shows the output of the two-way ANOVA test which examines the effect of age and genotype on PV count in the Subiculum. The table shows that at α = 0.05 the difference in PV count differs significantly by age, but not genotype.

	Df	Sum Sq	Mean Sq	F value	Pr(>F)
Age	1	210.5	210.5	7.071	0.0137
Genotype	1	1281.8	1281.8	43.062	8.70E-07
Age:Genotype	1	35	35	1.175	0.2891
Residuals	24	714.4	29.8		

Table A10. ANOVA output Corresponding to Figure 6C. The table above shows the output of the two-way ANOVA test which examines the effect of age and genotype on PNN count in the Subiculum. The table shows that at α = 0.05 the number of WFA+ PNNs in the Subiculum differs significantly by both age and genotype.

	Df	Sum Sq	Mean Sq	F value	Pr(>F)
Age	1	311	311	0.737	0.4
Genotype	1	3323	3323	7.875	0.01
Age:Genotype	1	138	138	0.327	0.573
Residuals	23	9703	422		

Table A11. ANOVA output Corresponding to Figure 7B. The table above shows the output of the two-way ANOVA test that examines the effect of age and genotype on % PV+ neurons associated with a PNN in the Subiculum. The table shows that at α = 0.05, the % of PV+ neurons associated with a PNN in the Subiculum differs significantly by genotype, but not age.

	Df	Sum Sq	Mean Sq	F value	Pr(>F)
Age	1	5462	5462	28.461	1.78E-05
Genotype	1	209	209	1.088	0.307
Age:Genotype	1	86	86	0.448	0.51
Residuals	24	4606	192		

Table A12. ANOVA output Corresponding to Figure 7C. The table above shows the output of the two-way ANOVA test that examines the effect of age and genotype on % PNNs associated with a PV+ neuron in the Subiculum. The table shows that at α = 0.05, the % of PNNs associated with a PV+ neuron in the Subiculum differs significantly by age, but not by genotype.

Appendix B: R Code used to Integrate and Analyze Data

Processing.R:

```
##Processing.R
library(tidyverse)
library(tiff)
library(ggplot2)
#Input parent directory
parent_dir <- "/Users/deborahnelson/Desktop/ImageJ_csv_manALL"
subfolders_age <- list.dirs(path = parent_dir, recursive = FALSE)
#Instantiates data frame. each row will be one individual brain
combined_df <- data.frame(ID = character(0), Age = character(0), Geno = character(0),+
                          ctx_PV = numeric(0), ctx_PNN = numeric(0), ctx_both = numeric(0))
colnames(combined_df) <- c("ID", "Age", "Geno", "back_PV", "back_PNN", "back_both", +
                           "front_PV", "front_PNN", "front_both", +
                           "postSub_PV", "postSub_PNN", "postSub_both",+
                           "sub_PV", "sub_PNN", "sub_both")
row <-0
# loop through subfolder for each age
for (subfolder_A in subfolders_age) {
  subfolders_Disease <- list.dirs(path = subfolder_A, recursive = FALSE)
  #loop through subfolder for each Genotype (WT and 5XFAD)
  for(subfolder_B in subfolders_Disease){
  subfolders_ID <- list.dirs(path = subfolder_B, recursive = FALSE)
  #loop through subfolders for each brain in the given category
  for(subfolder_C in subfolders_ID){
    row <- row +1
    #determine Age,Genotype, and "ID" for given brain
    long_Age <- unlist(strsplit(subfolder_A, "/"))
    Age <- tail(long_Age, n = 1)
    long_Disease <- unlist(strsplit(subfolder_B, "/"))
    Disease <- tail(long_Disease, n = 1)
    long_ID <- unlist(strsplit(subfolder_C, "/"))
    ID <- tail(long_ID, n = 1)
    #save characteristics in first three rows of a new column
    combined_df[row, 1:3] <- c(ID, Age, Disease)
    subfolders_region <- list.dirs(path = subfolder_C, recursive = FALSE)
    reg <-4
    #save pnn and pv data frame for each Brain
    for(subfolder_D in subfolders_region){
      csv_files <- list.files(path = subfolder_D, pattern = "*.csv", full.names = TRUE)
      for (csv_file in csv_files) {
        df <- read.csv(csv_file)
        df_list[[csv_file]] <- df
        if(grepl("WFA", csv_file))
          {pnn <- df}
        else
          {pv <- df}
      }
      #If at least on PV in given region, determine localization with PNNs
      if(nrow(pv)>0){
        pnn$pvMatch <-0
        pv$pnnMatch <- 0
      for (i in 1:nrow(pnn)){
        for(j in 1:nrow(pv)){
          if((abs(pnn$X[i]-pv$X[j]) <11) & (abs(pnn$Y[i]-pv$Y[j]) <11)){
            pnn$pvMatch[i] <- 1
            pv$pnnMatch[j] <-1
          }
        }
      }
     overlap <- sum(pv$pnnMatch ==1)
     #save number of pvs, number of pnns and percentage co-localization for each brain region, creating new columns for each
     combined_df[row, reg:(reg+4)] <- c(nrow(pv), nrow(pnn), overlap, (100*overlap/nrow(pv)), (100*overlap/nrow(pnn)) )}
     else{ combined_df[row, reg:(reg+4)] <- c(nrow(pv), nrow(pnn), sum(pnn$pvMatch ==1), NA, NA) }
    reg <- reg+5
  }
  }
  }
```

```r
}
#name columns
colnames(combined_df) <- c("ID", "Age", "Geno", "back_PV", "back_PNN", "back_both", "% PNN+ PVs (back)", +
                           "% PV+ PNNs (back)", "front_PV", "front_PNN", "front_both","% PNN+ PVs (front)", "% PV+ PNNs (fro
combined_df[3, 19:23] <- combined_df[3, 14:18]
combined_df[3, 14:18] <- NA
#output csv
write_csv(combined_df,  "/Users/deborahnelson/Desktop/ImageJ_csv_manALL/combined_man.csv")
combined_df$Age <- as.factor(combined_df$Age)
combined_df$Geno <- as.factor(combined_df$Geno)
library("ggpubr")
#boxplot and two way ANOVA for back PV count
ggboxplot(combined_df, x = "Age", y = "back_PV", fill = "Geno",
       palette = c("tomato", "steelblue1")) + ylab("PV Count (Post. Ctx.)") +
  ggtitle("Post.Ctx. PV Count by Genotype and Age")  + theme(legend.position="right") +
  theme(text = element_text(size=16)) + labs(color = "Mouse Model")
pv_back <- aov(back_PV ~ Age + Geno + Age:Geno, data = combined_df)
summary(pv_back)
#boxplot and two way anova for front PV count
ggboxplot(combined_df, x = "Age", y = "front_PV", fill = "Geno",
          palette = c("tomato", "steelblue1")) + ylab("PV Count (Ant. Ctx.)") +
  ggtitle("Ant. Ctx. PV Count by Genotype and Age")  + theme(legend.position="right") +
  theme(text = element_text(size=16)) + labs(color = "Mouse Model")
pv_front <- aov(front_PV ~ Age + Geno + Age:Geno, data = combined_df)
summary(pv_front)
#boxplot and two way anova for Subiculum PV count
ggboxplot(combined_df, x = "Age", y = "sub_PV", fill = "Geno",
          palette = c("tomato", "steelblue1")) + ylab("PV Count (Subiculum)") +
  ggtitle("Subiculum PV Count by Genotype and Age")  + theme(legend.position="right") +
  theme(text = element_text(size=16)) + labs(color = "Mouse Model")
pv_sub <- aov(sub_PV ~ Age + Geno + Age:Geno, data = combined_df)
summary(pv_sub)
#boxplot and two way anova for back PNN count
ggboxplot(combined_df, x = "Age", y = "back_PNN", fill = "Geno",
          palette = c("tomato", "steelblue1")) + ylab("WFA+ PNN Count (Post. Ctx.)") +
  ggtitle("Post.Ctx. PNN Count by Genotype and Age")  + theme(legend.position="right") +
  theme(text = element_text(size=16)) + labs(color = "Mouse Model")
pnn_back <- aov(back_PNN ~ Age + Geno + Age:Geno, data = combined_df)
summary(pnn_back)
#boxplot and two way anova for front PNN count
ggboxplot(combined_df, x = "Age", y = "front_PNN", fill = "Geno",
          palette = c("tomato", "steelblue1")) + ylab("WFA+ PNN Count (Ant. Ctx.)") +
  ggtitle("Ant. Ctx. PNN Count by Genotype and Age")  + theme(legend.position="right") +
  theme(text = element_text(size=16)) + labs(color = "Mouse Model")
pnn_front <- aov(front_PNN ~ Age + Geno + Geno:Age, data = combined_df)
summary(pnn_front)
#boxplot and two way anova for Subiculum PNN count
ggboxplot(combined_df, x = "Age", y = "sub_PNN", fill = "Geno",
          palette = c("tomato", "steelblue1")) + ylab("WFA+ PNN Count (Subiculum)") +
  ggtitle("Subiculum PNN Count by Genotype and Age")  + theme(legend.position="right") +
  theme(text = element_text(size=16)) + labs(color = "Mouse Model")
pnn_sub <- aov(sub_PNN ~ Age + Geno + Age:Geno, data = combined_df)
summary(pnn_sub)
#boxplot and two way anova for back %PNN+PVs
ggboxplot(combined_df, x = "Age", y = "% PNN+ PVs (back)", fill = "Geno",
          palette = c("tomato", "steelblue1")) + ylab("% PNN+ PVs (Post. Ctx.)") +
  ggtitle("Post.Ctx. % PNN+ PVs by Genotype and Age")  + theme(legend.position="right") +
  theme(text = element_text(size=16)) + labs(color = "Mouse Model")

pnnOnPV_back <- aov(`% PNN+ PVs (back)` ~ Age + Geno + Age:Geno, data = combined_df)
summary(pnnOnPV_back)
#boxplot and two way anova for front %PNN+PVs
ggboxplot(combined_df, x = "Age", y = "% PNN+ PVs (front)", fill = "Geno",
          palette = c("tomato", "steelblue1")) + ylab("% PNN+ PVs (Ant. Ctx.)") +
  ggtitle("Ant. Ctx. % PNN+ PVs by Genotype and Age")  + theme(legend.position="right") +
  theme(text = element_text(size=16)) + labs(color = "Mouse Model")
```

```
  theme(text = element_text(size=16)) + labs(color = "Mouse Model")
pnnOnPV_front <- aov(`% PNN+ PVs (front)` ~ Age + Geno + Age:Geno, data = combined_df)
summary(pnnOnPV_front)
#boxplot and two way anova for Subiculum %PNN+PVs
ggboxplot(combined_df, x = "Age", y = "% PNN+ PVs (Sub)", fill = "Geno",
          palette = c("tomato", "steelblue1")) + ylab("% PNN+ PVs (Subiculum)") +
  ggtitle("Subiculum % PNN+ PVs by Genotype and Age")  + theme(legend.position="right") +
  theme(text = element_text(size=16)) + labs(color = "Mouse Model")
pnnOnPV_sub <- aov(`% PNN+ PVs (Sub)` ~ Age + Geno + Age:Geno, data = combined_df)
summary(pnnOnPV_sub)
#boxplot and two way anova for back %PV+PNNs
ggboxplot(combined_df, x = "Age", y = "% PV+ PNNs (back)", fill = "Geno",
          palette = c("tomato", "steelblue1")) + ylab("% PV+ PNNs (Post. Ctx.)") +
  ggtitle("Post.Ctx. % PV+ PNNs by Genotype and Age")  + theme(legend.position="right") +
  theme(text = element_text(size=16)) + labs(color = "Mouse Model")

pvONPNN_back <- aov(`% PV+ PNNs (back)` ~ Age + Geno + Age:Geno, data = combined_df)
summary(pvONPNN_back)
#boxplot and two way anova for front %PV+PNNs
ggboxplot(combined_df, x = "Age", y = "% PV+ PNNs (front)", fill = "Geno",
          palette = c("tomato", "steelblue1")) + ylab("% PV+ PNNs (Ant. Ctx.)") +
  ggtitle("Ant. Ctx. % PV+ PNNs by Genotype and Age")  + theme(legend.position="right") +
  theme(text = element_text(size=16)) + labs(color = "Mouse Model")
pvONPNN_front <- aov(`% PV+ PNNs (front)` ~ Age + Geno + Age:Geno, data = combined_df)
summary(pvONPNN_front)
#boxplot and two way anova for Subiculum %PV+PNNs
ggboxplot(combined_df, x = "Age", y = "% PV+ PNNs (Sub)", fill = "Geno",
          palette = c("tomato", "steelblue1")) + ylab("% PV+ PNNs (Subiculum)") +
  ggtitle("Subiculum % PV+ PNNs by Genotype and Age")  + theme(legend.position="right") +
  theme(text = element_text(size=16)) + labs(color = "Mouse Model")
pvONPNN_sub <- aov(`% PV+ PNNs (Sub)` ~ Age + Geno + Age:Geno, data = combined_df)
summary(pvONPNN_sub)
```

Processing_Plaques.R

```r
library(tidyverse)
install.packages("tiff")
library(tiff)
library(ggplot2)
library(broom)
install.packages("popbio")
library(popbio)
#input parent directory
parent_dir <- "/Users/deborahnelson/Desktop/CTX_MAN"
PV_list <- list()
PNN_list <- list()
row_5xPV <-0
row_5xPNN <- 0
row_totPV <- 1
row_totPNN <- 1
subfolders_model <- list.dirs(path = parent_dir, recursive = FALSE)

#Instantiate data frames
plaq_pv <- data.frame(ID = numeric(0), Brain = numeric(0), PlaqDist = numeric(0), PlaqueSize = numeric(0),
plaq_pnn <- data.frame(ID = numeric(0), Brain = numeric(0), PlaqDist = numeric(0), PlaqueSize = numeric(0),

all_pv <- data.frame(Age = character(0), Geno = character(0), PNN = numeric(0))
all_pnn <- data.frame(Age = character(0), Geno = character(0), PV = numeric(0))

#for each Genotype subfolder
for (subfolder_A in subfolders_model) {
  long_Geno <- unlist(strsplit(subfolder_A, "/"))
  Geno <- tail(long_Geno, n = 1)
  subfolders_Age <- list.dirs(path = subfolder_A, recursive = FALSE)
  #for each Age subfolder within Genotype
  for(subfolder_B in subfolders_Age){
    long_Age <- unlist(strsplit(subfolder_B, "/"))
    Age <- tail(long_Age, n = 1)
    csv_files <- list.files(path = subfolder_B, pattern = "*.csv", full.names = TRUE)
    #load pnn and pv for each brain
    for (csv_file in csv_files) {
      df <- read.csv(csv_file)
      df_list[[csv_file]] <- df
      if(grepl("WFA", csv_file))
      {pnn <- df}
      else if (grepl("PV", csv_file))
      {pv <- df}
    }
    pv$pnnMatch <- 0
    pnn$pvMatch <- 0
    #assess colocalization between pv and pnn
    for (i in 1:nrow(pnn)){
      for(j in 1:nrow(pv)){
        if((abs(pnn$X[i]-pv$X[j]) <11) & (abs(pnn$Y[i]-pv$Y[j]) <11)){
          pv$pnnMatch[j] <-1
          pnn$pvMatch[i] <- 1
        }
      }
    }
    #add each individual pv and pnn to data frame
    for (i in 1: nrow(pv)){
      all_pv[row_totPV, 1:3] <- c(Age, Geno, pv$pnnMatch[i])
      row_totPV <- row_totPV +1
    }
    for (i in 1: nrow(pnn)){
      all_pnn[row_totPNN, 1:3] <- c(Age, Geno, pnn$pvMatch[i])
      row_totPNN <- row_totPNN +1
    }
    if(Geno == "5XFAD"){
      for (csv_file in csv_files) {
        df <- read.csv(csv_file)
```

```
        df_list[[csv_file]] <- df
        if(grepl("4G8", csv_file))
        {plaq <- df}
      }

      pv$plaqDist <- 10000
      pv$plaqSize <- 0
      pnn$plaqDist <- 10000
      pnn$plaqSize <- 0

      #adds row to exiting dataframe for each PV with its nearest plaque distance and size
      for(b in 1:nrow(pv)){
        row_5xPV  = row_5xPV  +1
        for (a in 1:nrow(plaq)){
          dist <- sqrt(sum(((plaq$X[a]-pv$X[b])^2) , ((plaq$Y[a]-pv$Y[b])^2)))

          if(dist< pv$plaqDist[b]){
            pv$plaqDist[b] <- as.numeric(dist)
            pv$plaqSize[b] <- as.numeric(plaq$Area[a])
          }
        }
        plaq_pv[row_5xPV ,1:2] <- c(row_5xPV , Age)
        plaq_pv[row_5xPV , 3:5] <- c(pv$plaqDist[b], pv$plaqSize[b], pv$pnnMatch[b])
      }
      #adds row to exiting dataframe for each PNN with its nearest plaque distance and size
      for(d in 1:nrow(pnn)){
        row_5xPNN = row_5xPNN +1
        for (c in 1:nrow(plaq)){
          dist <- sqrt(sum(((plaq$X[c]-pnn$X[d])^2) , ((plaq$Y[c]-pnn$Y[d])^2)))

          if(dist< pnn$plaqDist[d]){
            pnn$plaqDist[d] <- as.numeric(dist)
            pnn$plaqSize[d] <- as.numeric(plaq$Area[c])
          }
        }
        plaq_pnn[row_5xPNN,1:2] <- c(row_5xPNN, Age)
        plaq_pnn[row_5xPNN, 3:5] <- c(pnn$plaqDist[d], pnn$plaqSize[d], pnn$pvMatch[d])
      }
    }
  }
}
##Create Figure 8 and Table 1
all_pv$PNN <- as.numeric(all_pv$PNN)
prop_df <- aggregate(PNN ~ Age + Geno, data = all_pv, FUN = function(x) mean(x == 1))
ggplot(prop_df, aes(x = Age, y = PNN, fill = Geno)) +
  geom_bar(stat = "identity", position = "dodge") +
  labs(x = "Age", y = "% PNN+ PV interneurons", fill = "Mouse Model") +
  ggtitle("% PNN+ PV Neurons by Age and Model")
all_pv$PNN <- factor(all_pv$PNN)
all_pv$Geno <- factor(all_pv$Geno)
all_pv$Age <- factor(all_pv$Age)
logit_PV <- glm(PNN ~ Age + Geno +Age:Geno, data =all_pv, family = "binomial")
summary(logit_PV)

##Create Figure 9 and Table 2
all_pnn$PV <- as.numeric(all_pnn$PV)
prop_df <- aggregate(PV ~ Age + Geno, data = all_pnn, FUN = function(x) mean(x == 1))
ggplot(prop_df, aes(x = Age, y = PV, fill = Geno)) +
  geom_bar(stat = "identity", position = "dodge") +
  labs(x = "Age", y = "% PV+ PNNs", fill = "Mouse Model") + ggtitle("% PV+ PNNs by Age and Model")

all_pnn$PV <- factor(all_pnn$PV)
all_pnn$Geno <- factor(all_pnn$Geno)
all_pnn$Age <- factor(all_pnn$Age)
logit_PNN <- glm(PV ~ Age + Geno +Age:Geno, data =all_pnn, family = "binomial")
summary(logit_PNN)
```

```
134 ##Create Figure 10 and Table 3
135 plaq_pv$PNN <- as.factor(plaq_pv$PNN)
136 plaq_pv$Brain <- as.factor(plaq_pv$Brain)
137 logit_plaq_pv <- glm(PNN ~ PlaqDist + PlaqueSize + Brain + PlaqDist:PlaqueSize + PlaqDist:Brain +
138                       PlaqueSize:Brain , data = plaq_pv, family = "binomial")
139 summary(logit_plaq_pv)
140 logit_plaq_pv_simp <- glm(PNN ~ PlaqDist , data = plaq_pv, family = "binomial")
141 summary(logit_plaq_pv_simp)
142 library(popbio)
143 plaq_pv$PNN <- as.numeric(plaq_pv$PNN)-1
144 logi.hist.plot(plaq_pv$PlaqDist, plaq_pv$PNN, boxp = FALSE, type = "hist", col = "gray", +
145                 xlab = "Distance to Plaque", mainlabel = "Probability PV+ neuron being surrounded by a PNN
146 plaq_pv$PNN <- as.factor(plaq_pv$PNN)
147 levels(plaq_pv$PNN) <- c("No", "Yes")
148 ggplot(plaq_pv, aes(x=Brain, y= PlaqDist, fill= PNN )) +
149   geom_boxplot() + xlab("Age (mo)") + ylab("Distance to Plaque") +
150   ggtitle("PV distance to plaque by Age and PNN presence") + labs(fill = "PNN?") +
151   theme(text = element_text(size=16))
152
153
154 ##Create Figure 11 and Table 4
155 plaq_pnn$Brain <- as.factor(plaq_pnn$Brain)
156 plaq_pnn$PV <- as.factor(plaq_pnn$PV)
157 logit_plaq_pnn <- glm(PV ~ PlaqDist + PlaqueSize + Brain + PlaqDist:PlaqueSize + PlaqDist:Brain + PlaqueSiz
158 summary(logit_plaq_pnn)
159 logit_plaq_pnn_simp <- glm(PV ~ PlaqDist, data = plaq_pnn, family = "binomial")
160 summary(logit_plaq_pnn_simp)
161 plaq_pnn$PV <- as.factor(plaq_pnn$PV)
162 levels(plaq_pnn$PV) <- c("No", "Yes")
163 ggplot(plaq_pnn, aes(x=Brain, y= PlaqDist, fill=PV)) +
164   geom_boxplot() + xlab("Age (mo)") + ylab("Distance to Plaque") +
165   ggtitle("PNN distance to plaque by Age and PV presence") + labs(fill = "Associated PV?")
166 + theme(text = element_text(size=16))
```

References

'2020 Alzheimer's disease facts and figures'. 2020. *Alzheimers Dement*.

Allen, M., S. Ghosh, G. P. Ahern, S. Villapol, K. A. Maguire-Zeiss, and K. Conant. 2016. 'Protease induced plasticity: matrix metalloproteinase-1 promotes neurostructural changes through activation of protease activated receptor 1', *Sci Rep*, 6: 35497.

Baig, S., G. K. Wilcock, and S. Love. 2005. 'Loss of perineuronal net N-acetylgalactosamine in Alzheimer's disease', *Acta Neuropathol*, 110: 393-401.

Balmer, T. S. 2016. 'Perineuronal Nets Enhance the Excitability of Fast-Spiking Neurons', *eNeuro*, 3.

Banerjee, S. B., V. A. Gutzeit, J. Baman, H. S. Aoued, N. K. Doshi, R. C. Liu, and K. J. Ressler. 2017. 'Perineuronal Nets in the Adult Sensory Cortex Are Necessary for Fear Learning', *Neuron*, 95: 169-79 e3.

Bekku, Y., W. D. Su, S. Hirakawa, R. Fassler, A. Ohtsuka, J. S. Kang, J. Sanders, T. Murakami, Y. Ninomiya, and T. Oohashi. 2003. 'Molecular cloning of Bral2, a novel brain-specific link protein, and immunohistochemical colocalization with brevican in perineuronal nets', *Mol Cell Neurosci*, 24: 148-59.

Bosiacki, M., M. Gassowska-Dobrowolska, K. Kojder, M. Fabianska, D. Jezewski, I. Gutowska, and A. Lubkowska. 2019. 'Perineuronal Nets and Their Role in Synaptic Homeostasis', *Int J Mol Sci*, 20.

Braak, H., and E. Braak. 1991. 'Neuropathological stageing of Alzheimer-related changes', *Acta Neuropathol*, 82: 239-59.

Cabungcal, J. H., P. Steullet, H. Morishita, R. Kraftsik, M. Cuenod, T. K. Hensch, and K. Q. Do. 2013. 'Perineuronal nets protect fast-spiking interneurons against oxidative stress', *Proc Natl Acad Sci U S A*, 110: 9130-5.

Carulli, D., R. Broersen, F. de Winter, E. M. Muir, M. Meskovic, M. de Waal, S. de Vries, H. J. Boele, C. B. Canto, C. I. De Zeeuw, and J. Verhaagen. 2020. 'Cerebellar

plasticity and associative memories are controlled by perineuronal nets', *Proc Natl Acad Sci U S A*, 117: 6855-65.

Carulli, D., K. E. Rhodes, D. J. Brown, T. P. Bonnert, S. J. Pollack, K. Oliver, P. Strata, and J. W. Fawcett. 2006. 'Composition of perineuronal nets in the adult rat cerebellum and the cellular origin of their components', *J Comp Neurol*, 494: 559-77.

Carulli, D., and J. Verhaagen. 2021. 'An Extracellular Perspective on CNS Maturation: Perineuronal Nets and the Control of Plasticity', *Int J Mol Sci*, 22.

Chelini, G., H. Pantazopoulos, P. Durning, and S. Berretta. 2018. 'The tetrapartite synapse: a key concept in the pathophysiology of schizophrenia', *Eur Psychiatry*, 50: 60-69.

Chen, X., D. B. Cho, and P. C. Yang. 2010. 'Double staining immunohistochemistry', *N Am J Med Sci*, 2: 241-5.

Corvetti, L., and F. Rossi. 2005. 'Degradation of chondroitin sulfate proteoglycans induces sprouting of intact purkinje axons in the cerebellum of the adult rat', *J Neurosci*, 25: 7150-8.

Crapser, J. D., E. E. Spangenberg, R. A. Barahona, M. A. Arreola, L. A. Hohsfield, and K. N. Green. 2020. 'Microglia facilitate loss of perineuronal nets in the Alzheimer's disease brain', *EBioMedicine*, 58: 102919.

Deepa, S. S., Y. Umehara, S. Higashiyama, N. Itoh, and K. Sugahara. 2002. 'Specific molecular interactions of oversulfated chondroitin sulfate E with various heparin-binding growth factors. Implications as a physiological binding partner in the brain and other tissues', *J Biol Chem*, 277: 43707-16.

Dityatev, A., G. Bruckner, G. Dityateva, J. Grosche, R. Kleene, and M. Schachner. 2007. 'Activity-dependent formation and functions of chondroitin sulfate-rich extracellular matrix of perineuronal nets', *Dev Neurobiol*, 67: 570-88.

Eimer, W. A., and R. Vassar. 2013. 'Neuron loss in the 5XFAD mouse model of Alzheimer's disease correlates with intraneuronal Abeta42 accumulation and Caspase-3 activation', *Mol Neurodegener*, 8: 2.

Favuzzi, E., A. Marques-Smith, R. Deogracias, C. M. Winterflood, A. Sanchez-Aguilera, L. Mantoan, P. Maeso, C. Fernandes, H. Ewers, and B. Rico. 2017. 'Activity-Dependent Gating of Parvalbumin Interneuron Function by the Perineuronal Net Protein Brevican', *Neuron*, 95: 639-55 e10.

Frischknecht, R., M. Heine, D. Perrais, C. I. Seidenbecher, D. Choquet, and E. D. Gundelfinger. 2009. 'Brain extracellular matrix affects AMPA receptor lateral mobility and short-term synaptic plasticity', *Nat Neurosci*, 12: 897-904.

Gogolla, N., P. Caroni, A. Luthi, and C. Herry. 2009. 'Perineuronal nets protect fear memories from erasure', *Science*, 325: 1258-61.

Guimaraes, A., S. Zaremba, and S. Hockfield. 1990. 'Molecular and morphological changes in the cat lateral geniculate nucleus and visual cortex induced by visual deprivation are revealed by monoclonal antibodies Cat-304 and Cat-301', *J Neurosci*, 10: 3014-24.

Gunduz-Cinar, O., E. Brockway, L. Lederle, T. Wilcox, L. R. Halladay, Y. Ding, H. Oh, E. F. Busch, K. Kaugars, S. Flynn, A. Limoges, O. Bukalo, K. P. MacPherson, S. Masneuf, C. Pinard, E. Sibille, E. J. Chesler, and A. Holmes. 2019. 'Identification of a novel gene regulating amygdala-mediated fear extinction', *Mol Psychiatry*, 24: 601-12.

Hartig, W., K. Brauer, and G. Bruckner. 1992. 'Wisteria floribunda agglutinin-labelled nets surround parvalbumin-containing neurons', *Neuroreport*, 3: 869-72.

Hockfield, S., R. G. Kalb, S. Zaremba, and H. Fryer. 1990. 'Expression of neural proteoglycans correlates with the acquisition of mature neuronal properties in the mammalian brain', *Cold Spring Harb Symp Quant Biol*, 55: 505-14.

Howell, M. D., L. A. Bailey, M. A. Cozart, B. M. Gannon, and P. E. Gottschall. 2015. 'Hippocampal administration of chondroitinase ABC increases plaque-adjacent synaptic marker and diminishes amyloid burden in aged APPswe/PS1dE9 mice', *Acta Neuropathol Commun*, 3: 54.

Hylin, M. J., S. A. Orsi, A. N. Moore, and P. K. Dash. 2013. 'Disruption of the perineuronal net in the hippocampus or medial prefrontal cortex impairs fear conditioning', *Learn Mem*, 20: 267-73.

Javonillo, D. I., K. M. Tran, J. Phan, E. Hingco, E. A. Kramar, C. da Cunha, S. Forner, S. Kawauchi, G. Milinkeviciute, A. Gomez-Arboledas, J. Neumann, C. E. Banh, M. Huynh, D. P. Matheos, N. Rezaie, J. A. Alcantara, A. Mortazavi, M. A. Wood, A. J. Tenner, G. R. MacGregor, K. N. Green, and F. M. LaFerla. 2021. 'Systematic Phenotyping and Characterization of the 3xTg-AD Mouse Model of Alzheimer's Disease', *Front Neurosci*, 15: 785276.

Kim, H., S. Ahrlund-Richter, X. Wang, K. Deisseroth, and M. Carlen. 2016. 'Prefrontal Parvalbumin Neurons in Control of Attention', *Cell*, 164: 208-18.

Klimczak, P., A. Rizzo, E. Castillo-Gomez, M. Perez-Rando, Y. Gramuntell, M. Beltran, and J. Nacher. 2021. 'Parvalbumin Interneurons and Perineuronal Nets in the Hippocampus and Retrosplenial Cortex of Adult Male Mice After Early Social Isolation Stress and Perinatal NMDA Receptor Antagonist Treatment', *Front Synaptic Neurosci*, 13: 733989.

Kobayashi, K., P. C. Emson, and C. Q. Mountjoy. 1989. 'Vicia villosa lectin-positive neurones in human cerebral cortex. Loss in Alzheimer-type dementia', *Brain Res*, 498: 170-4.

Kochlamazashvili, G., C. Henneberger, O. Bukalo, E. Dvoretskova, O. Senkov, P. M. Lievens, R. Westenbroek, A. K. Engel, W. A. Catterall, D. A. Rusakov, M. Schachner, and A. Dityatev. 2010. 'The extracellular matrix molecule hyaluronic acid regulates hippocampal synaptic plasticity by modulating postsynaptic L-type Ca(2+) channels', *Neuron*, 67: 116-28.

Korotkova, T., E. C. Fuchs, A. Ponomarenko, J. von Engelhardt, and H. Monyer. 2010. 'NMDA receptor ablation on parvalbumin-positive interneurons impairs hippocampal synchrony, spatial representations, and working memory', *Neuron*, 68: 557-69.

Lendvai, D., M. Morawski, L. Negyessy, G. Gati, C. Jager, G. Baksa, T. Glasz, J. Attems, H. Tanila, T. Arendt, T. Harkany, and A. Alpar. 2013. 'Neurochemical mapping of the human hippocampus reveals perisynaptic matrix around functional synapses in Alzheimer's disease', *Acta Neuropathol*, 125: 215-29.

Meszar, Z., F. Girard, C. B. Saper, and M. R. Celio. 2012. 'The lateral hypothalamic parvalbumin-immunoreactive (PV1) nucleus in rodents', *J Comp Neurol*, 520: 798-815.

Miranda, J. M., E. Cruz, B. Bessieres, and C. M. Alberini. 2022. 'Hippocampal parvalbumin interneurons play a critical role in memory development', *Cell Rep*, 41: 111643.

Morawski, M., G. Bruckner, C. Jager, G. Seeger, and T. Arendt. 2010. 'Neurons associated with aggrecan-based perineuronal nets are protected against tau pathology in subcortical regions in Alzheimer's disease', *Neuroscience*, 169: 1347-63.

Morawski, M., S. Pavlica, G. Seeger, J. Grosche, E. Kouznetsova, R. Schliebs, G. Bruckner, and T. Arendt. 2010. 'Perineuronal nets are largely unaffected in Alzheimer model Tg2576 mice', *Neurobiol Aging*, 31: 1254-6.

Morikawa, S., Y. Ikegaya, M. Narita, and H. Tamura. 2017. 'Activation of perineuronal net-expressing excitatory neurons during associative memory encoding and retrieval', *Sci Rep*, 7: 46024.

Nahar, L., B. M. Delacroix, and H. W. Nam. 2021. 'The Role of Parvalbumin Interneurons in Neurotransmitter Balance and Neurological Disease', *Front Psychiatry*, 12: 679960.

Prince, M., G. C. Ali, M. Guerchet, A. M. Prina, E. Albanese, and Y. T. Wu. 2016. 'Recent global trends in the prevalence and incidence of dementia, and survival with dementia', *Alzheimers Res Ther*, 8: 23.

Prince, M., R. Bryce, E. Albanese, A. Wimo, W. Ribeiro, and C. P. Ferri. 2013. 'The global prevalence of dementia: a systematic review and metaanalysis', *Alzheimers Dement*, 9: 63-75 e2.

Reichelt, A. C., D. J. Hare, T. J. Bussey, and L. M. Saksida. 2019. 'Perineuronal Nets: Plasticity, Protection, and Therapeutic Potential', *Trends Neurosci*, 42: 458-70.

Romberg, C., S. Yang, R. Melani, M. R. Andrews, A. E. Horner, M. G. Spillantini, T. J. Bussey, J. W. Fawcett, T. Pizzorusso, and L. M. Saksida. 2013. 'Depletion of perineuronal nets enhances recognition memory and long-term depression in the perirhinal cortex', *J Neurosci*, 33: 7057-65.

Rupert, D. D., and S. D. Shea. 2022. 'Parvalbumin-Positive Interneurons Regulate Cortical Sensory Plasticity in Adulthood and Development Through Shared Mechanisms', *Front Neural Circuits*, 16: 886629.

Ruzicka, J., M. Dalecka, K. Safrankova, D. Peretti, P. Jendelova, J. C. F. Kwok, and J. W. Fawcett. 2022. 'Perineuronal nets affect memory and learning after synapse withdrawal', *Transl Psychiatry*, 12: 480.

Scarlett, J. M., S. J. Hu, and K. M. Alonge. 2022. 'The "Loss" of Perineuronal Nets in Alzheimer's Disease: Missing or Hiding in Plain Sight?', *Front Integr Neurosci*, 16: 896400.

Serrano-Pozo, A., M. P. Frosch, E. Masliah, and B. T. Hyman. 2011. 'Neuropathological alterations in Alzheimer disease', *Cold Spring Harb Perspect Med*, 1: a006189.

Shi, W., X. Wei, X. Wang, S. Du, W. Liu, J. Song, and Y. Wang. 2019. 'Perineuronal nets protect long-term memory by limiting activity-dependent inhibition from parvalbumin interneurons', *Proc Natl Acad Sci U S A*, 116: 27063-73.

Sorg, B. A., S. Berretta, J. M. Blacktop, J. W. Fawcett, H. Kitagawa, J. C. Kwok, and M. Miquel. 2016. 'Casting a Wide Net: Role of Perineuronal Nets in Neural Plasticity', *J Neurosci*, 36: 11459-68.

Sos, K. E., M. I. Mayer, V. T. Takacs, A. Major, Z. Bardoczi, B. M. Beres, T. Szeles, T. Saito, T. C. Saido, I. Mody, T. F. Freund, and G. Nyiri. 2020. 'Amyloid beta induces interneuron-specific changes in the hippocampus of APPNL-F mice', *PLoS One*, 15: e0233700.

Sparta, D. R., N. Hovelso, A. O. Mason, P. A. Kantak, R. L. Ung, H. K. Decot, and G. D. Stuber. 2014. 'Activation of prefrontal cortical parvalbumin interneurons facilitates extinction of reward-seeking behavior', *J Neurosci*, 34: 3699-705.

Subramanian, J., J. C. Savage, and M. E. Tremblay. 2020. 'Synaptic Loss in Alzheimer's Disease: Mechanistic Insights Provided by Two-Photon in vivo Imaging of Transgenic Mouse Models', *Front Cell Neurosci*, 14: 592607.

Suttkus, A., M. Morawski, and T. Arendt. 2016. 'Protective Properties of Neural Extracellular Matrix', *Mol Neurobiol*, 53: 73-82.

Suttkus, A., S. Rohn, C. Jager, T. Arendt, and M. Morawski. 2012. 'Neuroprotection against iron-induced cell death by perineuronal nets - an in vivo analysis of oxidative stress', *Am J Neurodegener Dis*, 1: 122-9.

Suttkus, A., S. Rohn, S. Weigel, P. Glockner, T. Arendt, and M. Morawski. 2014. 'Aggrecan, link protein and tenascin-R are essential components of the perineuronal net to protect neurons against iron-induced oxidative stress', *Cell Death Dis*, 5: e1119.

Tremblay, R., S. Lee, and B. Rudy. 2016. 'GABAergic Interneurons in the Neocortex: From Cellular Properties to Circuits', *Neuron*, 91: 260-92.

Ueno, H., K. Fujii, S. Suemitsu, S. Murakami, N. Kitamura, K. Wani, S. Aoki, M. Okamoto, T. Ishihara, and K. Takao. 2018. 'Expression of aggrecan components in perineuronal nets in the mouse cerebral cortex', *IBRO Rep*, 4: 22-37.

Vegh, M. J., C. M. Heldring, W. Kamphuis, S. Hijazi, A. J. Timmerman, K. W. Li, P. van Nierop, H. D. Mansvelder, E. M. Hol, A. B. Smit, and R. E. van Kesteren. 2014. 'Reducing hippocampal extracellular matrix reverses early memory deficits in a mouse model of Alzheimer's disease', *Acta Neuropathol Commun*, 2: 76.

Wingert, J. C., and B. A. Sorg. 2021. 'Impact of Perineuronal Nets on Electrophysiology of Parvalbumin Interneurons, Principal Neurons, and Brain Oscillations: A Review', *Front Synaptic Neurosci*, 13: 673210.

Yamada, J., T. Ohgomori, and S. Jinno. 2015. 'Perineuronal nets affect parvalbumin expression in GABAergic neurons of the mouse hippocampus', *Eur J Neurosci*, 41: 368-78.

Yau, J. O., C. Chaichim, J. M. Power, and G. P. McNally. 2021. 'The Roles of Basolateral Amygdala Parvalbumin Neurons in Fear Learning', *J Neurosci*, 41: 9223-34.